CHAPTER 5

Morphology of Crystalline Polymers and Methods for Its Investigation

5.1 Introduction

Polymers when they solidify will form a crystalline, partially ordered or totally disordered structure, depending on the regularity of the polymer backbone and the strength of the polymer–polymer interactions. In the melt, the flexible chain will normally contain a number of higher energy *gauche* conformations and adopts a *random* coiled form consistent with its inherent entropic disorder. On cooling, the lower energy *trans* form becomes predominant and chains prefer a more extended structure. The all-*trans* sequences produce linear sections of chain that are able to interact with other chains and initiate crystal growth. The extent to which the molecule eliminates the higher energy conformations on cooling will dictate its ability to crystallize. If the interactions opposing adoption of the *trans* conformation are insufficiently strong, then the disorder is retained in the solid state and an *amorphous* material is formed. For a polymer to exhibit crystallinity, the backbone structure must have a regular structure, strong interchain interactions or alternatively a specific chain conformation. The presence of chain stereochemical defects, e.g. atactic sequences and/or chain branches at high concentrations, makes it impossible for the polymer chain to form a close packed structure and an *amorphous* structure is formed. Large side chains will inhibit packing and promote *amorphous* structure formation. Specific interactions, such as hydrogen bonds or strong dipole–dipole interactions, may be sufficiently strong to create order between neighbouring polymer chains and promote microcrystal formation.

5.2 Crystallography and Crystallization

To help us understand the factors that influence crystal formation in polymers, it is appropriate to consider particular polymer systems.[1]

(a) Polyethylene

In Chapter 3 the basics of crystallography were introduced. Although polymers have long chains it is still possible to identify a unit cell that often corresponds to the monomer or groups of monomers and which is repeated in space. In the case of polymers, it is conventional to select the chain axis as the c-axis, except in the case of the monoclinic cell when the chain axis is the unique axis (b-axis).[1] A central postulate of polymer crystallography is that the polymer chains are in their lowest energy state. The most extensively investigated polymer system is polyethylene. As discussed in Chapter 1, the chain can exist in two conformations: the *trans* state that is the lowest energy state and a doubly degenerate higher energy *gauche* state. Despite the single lowest energy *trans* conformational structure, polyethylene shows two different crystal forms at normal pressure, pointing to the possibility that the all-*trans* chains may pack differently. Packing of the extended polyethylene chains will create a 'sheet' of molecules with a one-dimensional repeating structure. The next stack coming alongside the first will 'see' small differences in the potential energy surface, leading to a slightly displaced form of the normal packing of the chains. Because this potential surface contains only small differences in energy between similar states, more than one form is possible. The existence of more than one crystal form for a specific compound is referred to as *polymorphism*. For polyethylene, the orthorhombic structure shown in Figure 5.1 is the most stable. The all-*trans* backbone does not present a circular cross-section and the preferred packing is the orthorhombic structure. The deviation from the ideal hexagonal packing is not large. A monoclinic structure has been observed when crystallization occurs in stressed samples. When considering the crystallization process we must remember two factors: the odd–even effects in terms of the enthalpy of fusion (Chapter 1) and also the mobility of the alkane molecules in the plastic crystals (Chapter 4).

All these factors will influence the initial nucleation process and hence the form of the crystal structure that is observed.

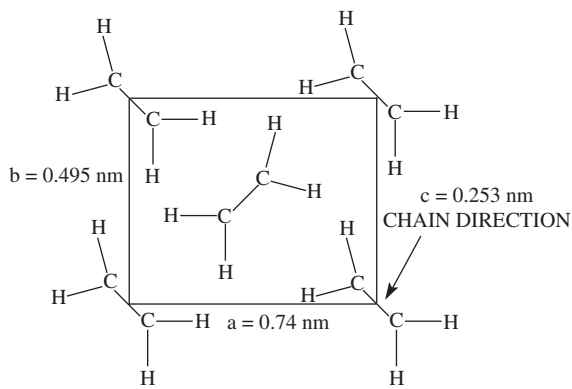

Figure 5.1 View along the c-axis, along the chain direction, for the orthorhombic polyethylene crystal.[1]

(b) Polypropylene

Whilst polyethylene with its simple regular structure is easy to visualize, forming an ordered crystalline structure, it is sometimes a little more difficult to appreciate the factors that influence crystallization in other polymer systems such as polypropylene. The methyl groups in the isotactic polymer would be expected to inhibit the packing of the chains; however, these groups impose a helical twist on the backbone and crystallization can occur (Figure 5.2).

X-Ray analysis indicates that fibres have a monoclinic unit cell structure containing 4 chains and 12 monomer units and cell parameters $a = 6.65$ Å, $b = 20.96$ Å, $c = 6.50$ Å, $\beta = 99.4°$. This structure is consistent with the chains having a three-fold helical conformation: 3_1 helix. The helical structures can register and pack to form a regular crystal structure. In contrast, the atactic material does not form a helical structure and crystallization is inhibited. As a consequence, atactic polypropylene is a soft flexible solid and is used as an additive to lubrication oils, whereas the isotactic polymer is rigid and used for fabrication of hot water pipes used in plumbing applications. Isotactic polypropylene has two helical forms, both having the same energy. The torsion angle about the $[–CH_2–CH[CH_3]–]_n$ bond is denoted ϕ_1 and the torsion angle associated with the $[–CH[CH_3]–CH_2–]$ bond is denoted ϕ_2. The two low-energy conformational states are repeats of $\phi_1 = 120°$, $\phi_2 = 0°$ (right-handed helical structure) and $\phi_1 = 0°$, $\phi_2 = 240°$ (left-handed helical structure). The isotactic polymer is a chiral molecule and hence can be either right or left handed. In the isotactic crystal of polypropylene there are four different possible helices: a right-handed helix pointing upwards and another pointing downwards and a complementary pair of left-handed helices. Although at first sight the upward and downwards helices would appear the same, a closer inspection indicates that they are different. It is therefore not surprising that isotactic polypropylene exhibits a number of polymorphs, referred to as α, β and γ forms. Packing adjacent chains with opposite senses of the helices creates the α form of isotactic polypropylene. In fact, it is generally found that the packing helices of an opposite form are better than if the same forms are used. The γ structure was first discovered in high-pressure crystallized isotactic polypropylene and X-ray

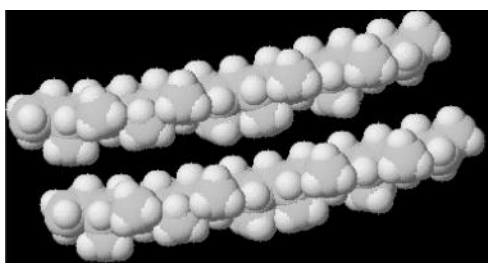

(a)

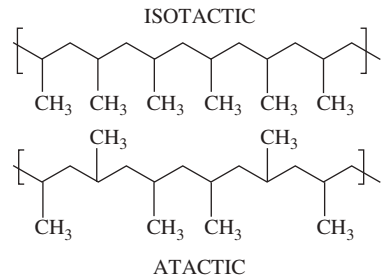

(b)

Figure 5.2 A space filling model of the isotactic structure of polypropylene (a) and symbolic structures for the polymers (b).

analysis suggests a triclinic structure with $a = 0.854$ nm, $b = 0.993$ nm and $c = 4.241$ nm.[2] If we compare these dimensions to those of the individual chains it becomes clear that the best fit of the structure is achieved with a structure in which alternative layers are each two chains thick, and with each of the bilayers at an angle of 80 ° to the adjacent bilayers.

The β form is a hexagonal form and produces spherulitic structure and is usually induced using nucleating agents. In addition to these three crystalline forms, isotactic polypropylene can exhibit a so-called smectic or mesomorphic phase on rapid cooling. An X-ray scattering pattern with two broad peaks centred at 14.8 ° and 21.2 ° (2θ, Cu K_α) showed that the density of this phase was 880 kg m^{-3}, compared with the density of 850 kg m^{-3} for the fully amorphous polypropylene[3] and it has been suggested that this corresponds to a *smectic* phase built up from bundles of straight chains of left- and right-handed helices with less than perfect order in the direction perpendicular to the chain helix axis.

(c) Polyoxymethylene

Replacement of one of the methylene groups of polyethylene by an oxygen creates polyoxymethylene. In this molecule, the lone pairs of electrons on the oxygen will interact with the hydrogen atoms on the adjacent carbon atoms and the preferred conformation is the nearly all-*gauche* structure which produces a stable trigonal form (I) and a less stable orthorhombic form (II). The unit cell contains chains with the same handedness, left and right-handed molecules appearing in different crystal lamellae.

(d) Poly(ethylene oxide)

In the crystalline state, the poly(ethylene oxide) chains form a structure which has seven monomer elements; $–(CH_2CH_2O)_n–$ and two helical turns per unit cell. The crystallographic unit cell contains four molecular chains and is monoclinic with $a = 7.96$ Å, $b = 13.11$ Å, $c = 1939$ Å and $\beta = 124.8$ °.[4–6] The chains have dihedral symmetry, two fold axes, one passing through the oxygen atoms and the other bisecting the carbon–carbon bond. The chain conformation assigned to internal rotation about the $–O–CH_2–$, $–CH_2–CH_2–$ and $–CH_2–O–$ bonds is *trans*, *gauche*, *trans* respectively. Although poly(ethylene oxide) is essentially very similar to polyethylene, it is therefore quite surprising the complexity of the chain conformation found in the solid and reflects the dominance of the local interactions in determining the unit cell structure.

Many isotactic forms of polymers or simple linear chains, such as polytetrafluoroethylene and poly(vinylidene chloride), have helical conformations. The pitch of the helix is determined by the influence of the nonbonding short-range interactions between adjacent atoms on the polymer backbone. Helical structures are frequently observed and reflect the subtle effects of these interactions.[7] The controlling factor is the enthalpy of the melt process and Table 5.1 summarizes values for some common polymer systems.

These polymers illustrate the complexity of predicting the crystal structure of these polymers. Although polystyrene, with its bulky phenyl side group, is normally considered to be an amorphous polymer, the isotactic form of the polymer forms a helix and a crystalline structure. Usually the density of the

Table 5.1 Heats of fusion, melting points and densities for some common polymers.

Monomer unit	*Enthalpy of fusion, ΔH ($J\ g^{-1}$)*	*Melt temperature (°C)*	*Density ($g\ cm^{-3}$)*	
			Amorphous	*Crystalline*
Ethylene (linear)	293	141	0.853	1.004
Propylene (isotactic)	79	187	0.853	0.946
Butene (isotactic)	163	140	0.859	0.951
4-Methylpentenene-1 (isotactic)	117	166	0.838	0.822
Styrene (isotactic)	96	240	1.054	1.126
Butadiene (1,4 polymer) (*cis*)	171	12	0.902	1.012
Butadiene (1,4 polymer) (*trans*)	67	142	0.891	1.036
Isoprene (1,4 polymer) (*cis*)	63	39	0.909	1.028
Isoprene (1,4 polymer) (*trans*)	63	80	0.906	1.051
Vinyl chloride (syndiotactic)	180	273	1.412	1.477
Vinyl alcohol	163	2165	1.291	1.350
Ethylene terephthalate	138	280	1.336	1.514
ε-Caprolactone	142	64	1.095	1.184
Ethylene oxide	197	69	1.127	1.239
Formaldehyde (oxymethylene)	326	184	1.335	1.505
Nylon 6	230	270	1.090	1.190
Nylon 6,6	301	280	1.091	1.241

crystalline form is higher than that of the amorphous solid; however, in the case of 4-methylpentenene-1 the reverse is the case. The crystal of 4-methylpentenene-1 has a 7_2 helix and this occupies a large volume leaving a hollow cylinder down the centre of the coil. Although nylon 6 and nylon 6,6 have similar melting temperatures they have significantly different enthalpies that reflects the differences in the hydrogen bonding in the two polymers and explains the significant difference in their densities and susceptibilities to moisture uptake.

In general, however, identification of the crystal cell is only part of the problem of characterizing the structure of crystalline polymers. Crystals are never perfect and the units cells do not infinitely duplicate through space even when they are grown very carefully from dilute solution using low molecular mass materials. As with the organic crystals considered in Chapter 3, a variety of defects can be observed and are associated with chain ends, kinks in the chain and jogs (defects where the chains do not lie exactly parallel). The presence of molecular (point) defects in polymer crystals is indicated by an expansion of the unit cell as has been shown by comparison of branched and linear chain polyethylene. The *c* parameter remains constant, but the *a* and *b* directions are expanded for the branched polymer crystals. Both methyl and

ethyl branches induce expansion, whereas larger pendant groups, propylene or longer homologues, are largely excluded from the crystals.

5.3 Single Crystal Growth

Our knowledge of the structure of crystalline polymers relies on a very large volume of research carried out on the crystal growth of polymers from dilute solution.[8–12] The majority of the early research focused on polyethylene and involved crystallization from 0.01% solutions in xylene. This method of crystal growth produces single crystals that are 10 nm thick platelets. In order to explain the shapes of these single crystals it was necessary to propose that the long polymer chains folded back and forward rather than being infinitely extended in space. Storks[13] proposed folding of polymer chains in *trans*-polyisoprene. An example of a transmission electron micrograph[12] showing that the crystals of polyethylene have a regular shape which are pyramidal in form is shown in Figure 5.3. Considering the polyethylene chains to be predominantly in an extended *trans* form, then the thickness of the platelets, ~ 10 nm, can only be explained by assuming that in some way the chains of the polymer fold back on themselves.

Careful examination of single crystals grown from solution at 70 °C in xylene indicated that they are lozenge shaped and have surfaces that are {110} planes.

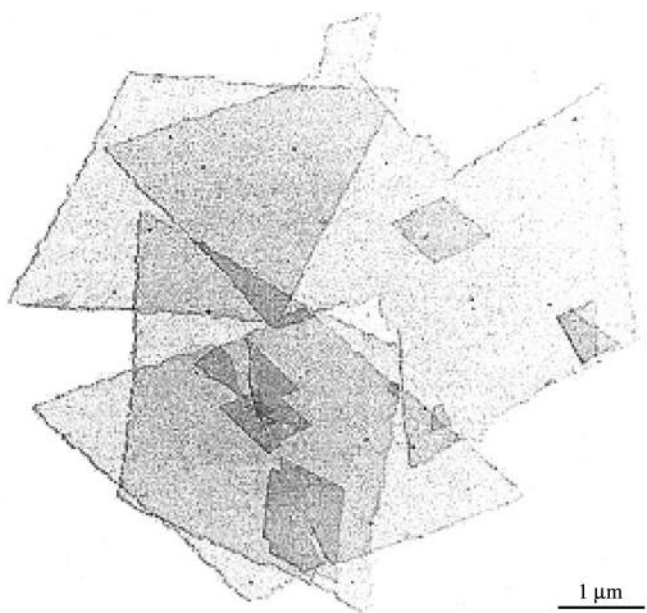

Figure 5.3 Transmission electron micrograph of a solution-grown single crystal of linear polyethylene showing lozenge-shaped crystals.[12]

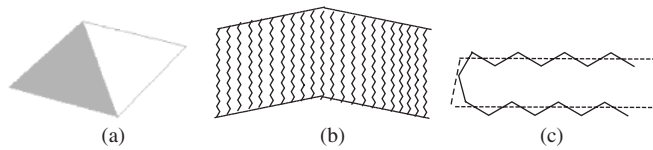

Figure 5.4 Chain packing to form pyramidal-shaped single crystal of polyethylene: (a) pyramidal shape; (b) chain alignment within pyramid; (c) close-up of the (110) chain fold with chain axes parallel but slightly displaced and the resulting inclined edge.

Crystals grown at 80 °C are truncated with two new sectors with {100} facets. The existence of crystallographic facets indicates that the growth process is controlled and that the chains are deposited in a regular manner. It must be recognized that the higher the temperature used for the growth, the greater will be the frequency of the higher energy *gauche* sequence in the chain. It is possible to rationalize the observed effects in terms of the conformation of the polymer chain in solution. In the {110} sectors, the folds of the chain lie along the [110] direction, whereas for {100} sectors, the chain folding is expected to occur along [010]. The difference in fold types affects the thermal stability of the sectors and it is noted that {100} sectors possess a lower melting point than the {110} sectors.

The single crystal images are obtained by lifting the crystal from the solution using a supporting metal grid. Corrugations of the crystal are sometimes observed and are a consequence of collapse of the pyramidal single crystals. The hollow pyramid shape arises from the chain axis not being parallel with the normal to the lamella direction. The chain axis is often found to be at an angle of $\sim 30^\circ$ with respect to the normal of the lamella and the tilt is a consequence of a small vertical displacement when the chains fold (Figure 5.4).

Similar displacements to those shown in Figure 5.4 are found in many types of crystal and indicate that the (110) fold is consistent with the chains being placed on a diamond lattice structure. The pyramidal crystal arises from the regular chain folding and constraints of the (110) fold. Further studies[13] have shown that the fold surfaces in the {110} sectors were parallel to the {312} planes and that the fold surfaces in the {100} sectors were parallel to {201} planes. A match between {312} and 201} is obtained only for certain fixed ratios of {100} and {100} growth.[14] A preference for such a growth ratio and deviations from this ideal shape may occur and are associated with distortions of the lattice. Crystals grown from the melt exhibit similar structure with a rooftop shape and has implications for the alignment of crystalline polymers when the melt is drawn below the melt temperature.[15]

5.3.1 Habit of Single Crystals

As with simple organic crystals, the temperature at which crystallization occurs will influence the habit of the crystal formed. Whereas in simple organic crystals the growth can be envisaged as occurring from the primary unit cell, in the case

of a polymer system the nucleus is formed by the alignment of sections of all-*trans* or similar chain structures. The conformational entropy of the polymer molecule in the melt will influence the length of these low-energy sections. The higher the temperature the more frequent the occurrence of the *gauche* sequences and the larger the B/A ratio with the consequence that a rounding of the crystal {100} surface occurs[16] (Figure 5.5). At the melt temperature, 130 °C, only a very small part of the periphery of the crystal lamellae is {110} facets, the remaining parts being rounded {100} surfaces. The variation in the shape, or *habit*, of the crystals is a direct reflection of the influence of chain folding on the growth mechanism. The changes in shape follow a smooth variation and the ratio B/A follows a continuous function with temperature. Crystals with well-defined {100} and {100} facts are typical of the crystallization of polyethylene at relatively low temperatures, 70 and 90 °C, from *p*-xylene.

Despite the apparent complexity of the growth behaviour of polyethylene, a number of characteristic shapes have been identified for particular polymer systems (Table 5.2).

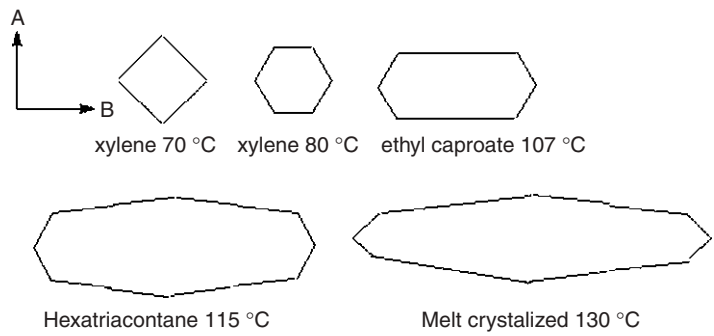

Figure 5.5 Schematic of the change of crystal shape with growth temperature for polyethylene obtained from different solvent systems.[15,16]

Table 5.2 Characteristic shapes for some polymer crystals grown from dilute solution.

Polymer	*Characteristic shape of crystal*
Polyoxymethylene	Hexagonal hollow pyramid
Poly(4-methyl-1-pentane) (isotactic)	Square-based pyramid
Polytetrafluoroethylene	Irregular hexagonal platelets
Poly(but-1-ene)	Square or hexagonal platelets
Polystyrene (iostactic)	Hexagonal platelets
Poly(ethylene oxide)	Square or hexagonal platelets
Poly(ethylene terephthalate)	Flat ribbons of ~30 nm width
Polyamide 6	Lozenge-shaped lamellae
Polyamide 6,6	Irregular hexagonal platelets tending to flat ribbons
Polypropylene (isotatic)	Lath shaped platelets

Most polymer crystals will exhibit facets and some like polyoxymethylene form hollow pyramids. The occurrence of the hollow pyramid is for similar reasons to that proposed for polyethylene and is a direct consequence of the constraints on the chain folding. The smooth surfaces observed for many crystal systems are evidence of regular chain folding, but are not proof that this occurs.

As in the case of simple crystals discussed in Chapter 2, spiral growth can be observed stemming from dislocations. The same factors appear to operate, except that now the step size is controlled by the lamellae thickness rather than the single atom attachment.

5.4 Crystal Lamellae and Other Morphological Features

5.4.1 Solution-Grown Crystals

If crystallization is carried out slowly in dilute solution then during lamellae growth, additional layers may be formed through the action of screw dislocations. When growth is slow the number of such defects is small and well-ordered multilayered crystals are formed. If, however, the growth rate is fast then complex lamellae aggregates that are either sheaf-like or spherical in outline are formed. The nature of these aggregates is very important as they can have profound effects on the mechanical properties of the resultant bulk solid. During the melt crystallization process, the shorter chains are rejected and become concentrated between the spherulites.[17] As such, interspherulitic regions constitute sites of potential weakness and are the location for crack propagation and dielectric breakdown. For this reason the spherulitic size and form are important in determining bulk polymer properties.

Whilst much of the initial research has focused on the structures generated from crystals grown from solutions of 0.01–0.001 wt%, it is the solid-phase morphology that is the more challenging to understand. A quantitative discussion of crystallization from dilute solution is attempted in Chapter 6; as an introduction, the factors that influence crystallization will be considered.

5.4.2 Chain Folding

A common feature of most polymer crystals is chain folding to form the lamellae and is observed in both solution-grown crystals and those obtained from the melt. One of the questions which arise when one considers chain folding is whether the folds are tight, occurring within four or so main-chain atoms, or loose and extending over many more. Although there may be complete folding in solution-grown single crystals, in the bulk a proportion of the molecules in adjacent lamellae must pass from one lamella to the next, *tie molecules*, and/or fold back into the lamellae from which they originate. Many mechanical properties are determined by the connectivity between the lamella structures and rely on the tie molecules to transfer the stress.

5.4.3 Crystal Habit

As indicated above, a wide variety of *habits* are found in solution-grown polymer crystals. Although it is possible to identify the 'ideal' crystal habit, it is also often found that in addition to the general rounding of the crystal faces, twinning of crystals can occur with the result that objects with six arms are common for {110} because (110) and $(1\bar{1}0)$ faces are inclined at 67.5°, close to 60°. Moreover, lath-type structures are prone to develop with twin boundaries along their centre lines because of the accelerated growth provided by the notch at the tip, which aids molecular attachment.[18,19] This is a similar effect to that observed in small-molecule crystals where defects form the sites for rapid growth.

5.4.4 Sectorization

Polymers are long chains and so far in the discussion there has not been obvious evidence of the effects of chain length on the crystal structure, chain folding, removing the obvious effects of the chain length. However, sectorization is the first effect that can be related to the length of the polymer chains. It is observed as a surface texture in which the lamellae are divided into discrete regions bounded by a growth face. This phenomenon is a direct consequence of chain folding along the growth face and would not occur if the chain formed pre-folded blocks before attachment to the crystal. Sectorization arises because folding of the chains transforms a long molecule into a pleated sheet which can extend across several successive lattice planes but essentially lies along the relevant growth surface denoted the *fold* plane.[20] The so aligned chain breaks the symmetry and slightly distorts the repetitive unit of chain packing within the lamellae. The fold plane in a given sector differs from nominally equivalent ones along which there is no folding and so transforming single lamellae into a multiple twin. A four-sided polyethylene lozenge (Figure 5.5) bounded by four {110} growth surfaces is, accordingly, a four-fold twin with four equivalent sectors in each of which the two nominally equivalent {110} surfaces will be parallel to the fold plane, the other is not. At higher growth temperatures lozenges become six sided with truncating {100} surfaces, and then there are six corresponding sectors. The two new ones denoted {100} sectors are twinned with respect to each other but are different in character from the four twinned {110} sectors and have a lower melting point. The size of the sector is governed by that of its growth face and can be very small, e.g. dendritic growth, when individual facets, each of which has its own micro-sector, may be as little as 20 nm wide.

5.4.5 Non-planar Geometries

One consequence of the distortions which are associated with the sectorization is to make the lamellae non-planar. Folding along the growth faces makes nominally equivalent planes in the subcell become non-equivalent adopting

slightly different spacings. For the three systems in which measurements have been reported, polyoxymethylene, isotactic poly(4-methylpent-1-ene)[21] and low molar mass polyethylene[22] which have, respectively, hexagonal, tetragonal and orthorhombic subcells, the distortion reported is of the order of ~ 0.001 nm. As a consequence, the transverse axes of the subcell no longer meet at precisely 60° or 90° and distortion of the crystal results. Such small effects are probably universal in sectored polymer lamellae. The pyramidal structures identified in Figure 5.4 can invert and appear as chair crystals or form derivative structures such as half hollow pyramidal/half ridged lamellae with a central hollow pyramidal portion.

5.5 Melt Grown Crystals

5.5.1 Melt-Crystallized Lamellae

Development of various specimen preparation methods[20] has allowed some important features for melt crystallization to be identified. It is found that the bulk material is full of lamellae that often have different profiles.[23] In a typical crystalline polymer, such as polyethylene, spherulitic growth is responsible for the spatial variation in physical properties. The structures that are observed are the results of the growth of dominant lamellae that branch and diverge. The space created between the lamellae is, except in the case of very low molecular weight materials, filled by *subsidiary* or *infilling* lamellae. This type of growth will produce lamellae with different characteristics for two reasons. Firstly, fractional crystallization in which the chains with different molar mass (chain length) segregate from one another allows the shorter chains to form lamellae which have a lower modulus and melting point. Secondly, the different orientations of the lamellae help to develop isotropic properties, a proportion of the lamellae being in the direction of the applied force and a proportion being perpendicular with a statistical distribution being in all other directions. If the material is cold drawn, then the applied stresses will develop physical characteristics in the material that are the result of alignment of the dominant lamellae and the development of an enhanced modulus in the draw direction. The natural draw ratio is influenced by the 20° alignment of the subsidiary lamellae to the dominant structures.

Changes in growth temperature can lead to the profile of the lamellae varying from planar to S or C shaped. The change in shape to an S profile {201} fold structure occurs at a critical growth rate and decreases for longer and/or more branched molecules.[24,25] The time taken for a single 5 nm thick molecule layer to be added to the crystal is $\sim 10^{-1}$ s for linear polyethylene of 100 000 molecular mass. For slower growth, {201} surfaces occur and nucleate as such, in contrast to faster growth, when lamellae nucleate with {001} surfaces and subsequently transform behind the growth front, adopting S profiles and thickening isothermally. For slower growth a molecule is able to achieve inclined fold packing as it adds to the crystal, but not for faster growth when

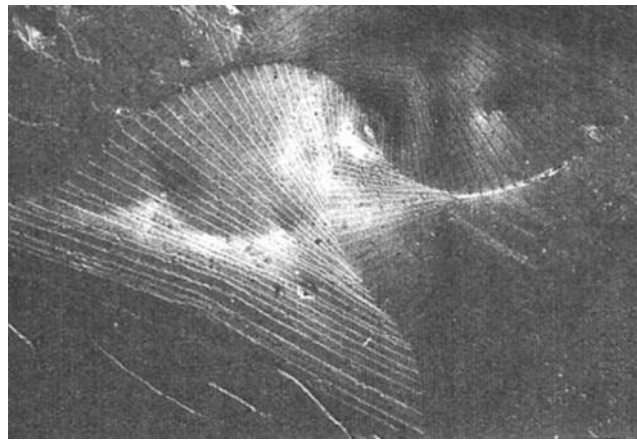

Figure 5.6 Electron micrograph of a multilayered crystal of polyethylene displaying regular rotation of successive growth terraces.[26]

improvements in fold packing must be accomplished within the constraints of surrounding lamellae. When a region of inclined packing is produced in the central part of the lamellae, *i.e.* the oldest portion of the lamellae, this leads automatically to an S profile in cross-section. Once more the habit can be significantly influenced by the occurrence and distribution of defects in the lamellae surface.

Keller[26] has shown that a terrace-like structure is observed reflecting the stacking of the lamellae structure in a melt-grown crystal (Figure 5.6).

5.5.2 Polymer Spherulites

The supermolecular structure exhibited by many polymers has features that are in the range of 0.5 μm to several millimetres. Such features can be observed using polarized light optical microscopy. The common form of structure observed is called a spherulite and, as its name implies, it is a circular crystalline object. The first spherulites found were in vitreous igneous rocks and the name comes from the Greek word for a ball or globe. A spherulite is an 'object' with spherical optical symmetry. Two unique refractive indices may be determined, namely the tangential (n_t) and radial (n_r) refractive indices. As an example, consider crystalline polyethylene. The single crystal or any orientated structure of this polymer may be considered to be uniaxially birefringent, with the unique direction (largest refractive index) along the chain axis—down the *stem*. Negative spherulites with $n_t > n_r$ have a higher proportion of the chains in the circumferential planes than along the radius of the spherulites. The direction of growth of polyethylene spherulites is always close to [010], *i.e.* the radius of the spherulite is parallel to the crystallographic b-axis (Figure 5.7).

Other polymers have other growth directions, e.g. monoclinic isotatic polypropylene grows faster along the a-axis. Similar behaviour is observed with

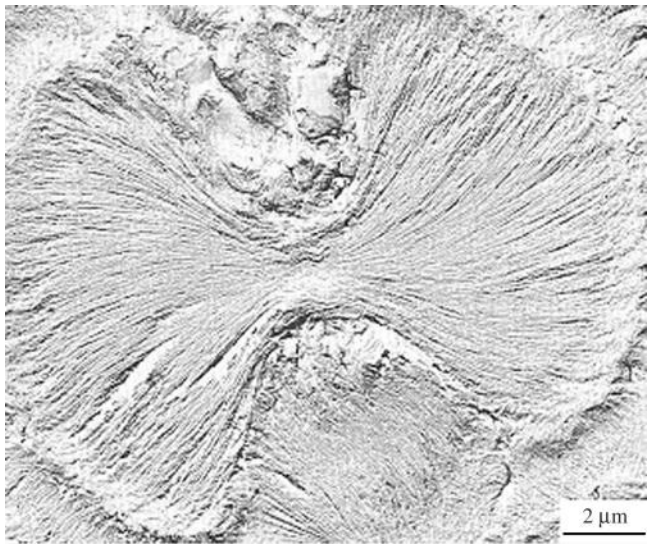

Figure 5.7 Sheaf-like lamellar aggregates crystallized from the melt in a blend of linear and low-density polyethylene at 125 °C.[27]

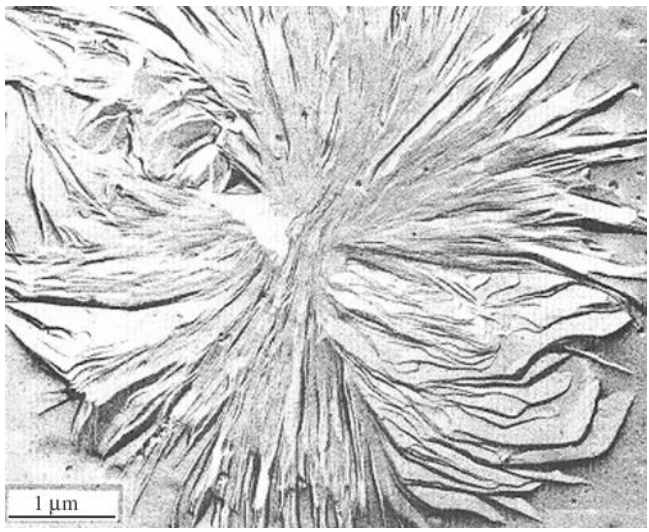

Figure 5.8 Micrograph of isotactic polystyrene crystallized at 200 °C showing sheaf-like spherulites.[27]

isotactic polystyrene crystallized at 200 °C that shows the characteristic sheaf-like spherulite structure (Figure 5.8). The size of the spherulites is controlled by the nucleation process which is almost invariably heterogeneous, *i.e.* growth starts from extraneous material such as dust or residual catalyst particles. Most

of the information on bulk structure has been obtained either from fracture surfaces or strained microtomed thick sections of polymer. As a result, the structures that are observed are never as clear and definitive as those for solution-grown single crystals. It is generally agreed, however, that spherulitic structure is controlled by the dominant lamella growth that usually adopts a circular format. Starting from an individual lamella, the growth progression is to first create the dominant lamellae that then create a multilayered axialite, a parallel organized set of lamellae. Out of this axialite will emerge several fast growing lamellae that may splay and present a sheaf-like appearance down the principal axis of the splay (Figures 5.7 and 5.8). From these splays will emanate lamellae which will eventually be at right angles to the original axis as well as growth occurring parallel to the original structures. A schematic representation is shown in Figure 5.9. The axialite is a non-spherical and irregular superstructure. Axialites are primarily found in low molar mass polyethylene at essentially all crystallization temperatures and in intermediate molar mass polyethylene crystallized at higher temperatures at undercooling less than 17 K.

Very high molar mass samples, typically with molar mass of 10^6 g mol^{-1} or greater, form so-called random lamellar structures. The entanglement effect is so extensive that the crystalline mass becomes very low and regular lamellar stacking is absent in these samples.

The gross morphology is a consequence of the intersection of the growth fronts from the various nucleation centres and the boundaries are often hyperbolic reflecting the intersection of the spherical structures. It must always be remembered that these are three-dimensional structures and apparently distorted shapes are often structures viewed at a different angle. All the structures in Figure 5.9b are created by rotation or skewing of the original spherulite (Figure 5.9a). When viewed with polarized light, a Maltese cross structure is usually observed and spherulites appear to have different shades. This behaviour is exemplified in the case of the optical microscopic images for ethylene–propylene shown in Figure 5.10.

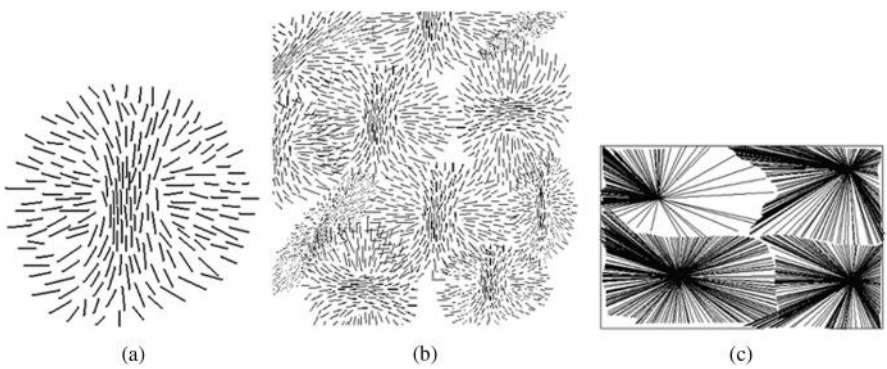

Figure 5.9 Schematic of lamellae growth (a) from an axialite to a spherulite and (b) packing into a solid. (c) Schematic of spherulites viewed with polarized light.

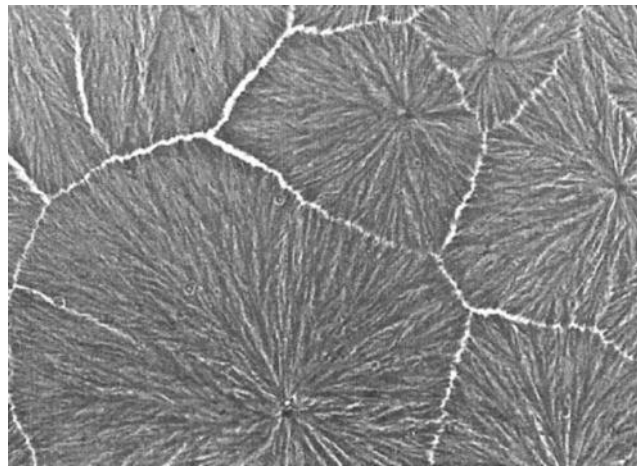

Figure 5.10 Optical micrograph of the spherulites produced by a propylene–ethylene copolymer.[28]

A scanning electron micrograph of a fracture surface of polypropylene shows the characteristic rings of an underlying spherulitic structure[29] (Figure 5.11). The spherulitic crystal structure can be subjected to low-temperature drawing. During this process the lamellae remain intact but are rotated into the line of the applied stress. As a consequence the lines of weakness that are the points at which the spherulites intersect open and form voids between the developing fibres. The spherulites elastically respond up to $\sim$30% strain, followed by permanent inhomogeneous changes which involve combinations of slip, twinning and phase changes.

The morphologies discussed so far have all been formed from isotropic melts. In practice melts are often subjected to shear forces and this can induce alignment in the chains, which aids crystallization in particular directions. Orientation of the melt causes an increase in the free energy and this itself constitutes an important factor in practical processing. Shish-kebabs[30] are formed from solutions that are subjected to elongational flow, which induces orientation of the solute molecules (Figure 5.12).

A central core of orientated bundles of fibres is formed at first as a direct consequence of the orientation. The shish-kebab structure consists of a central group of highly orientated fibrils from which lamellar crystals can grow and form the kebab structures (Figure 5.12). The central fibrils are formed from high molar mass material. Similar structures have been obtained during extrusion/injection moulding of the melt when extreme conditions are used and the melt is subjected to high elongational flow in combination with a high pressure or a high cooling rate. The orientated melt solidifies in a great many fibrous crystals from which lamella overgrowth occurs. The radiating lamellae nucleating in adjacent fibrils are interlocked, a fact that is considered to be important for the superior stiffness properties of the melt-extruded fibres. The fibrillar structure is present in ultra-orientated samples. It consists of highly

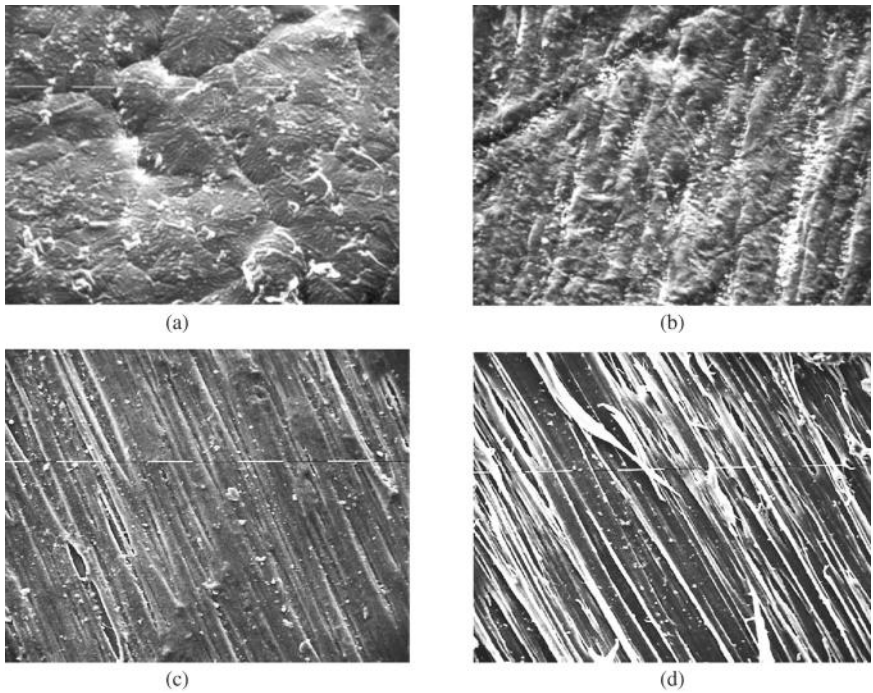

Figure 5.11 Scanning electron micrographs of the fracture surfaces of undrawn (a) and drawn (b), $\lambda = (l/l_0) = 2.6$; (c) $\lambda = 6$; (d) $\lambda = 14$ (where l is the drawn length and l_0 is the undrawn length of the sample).[29]

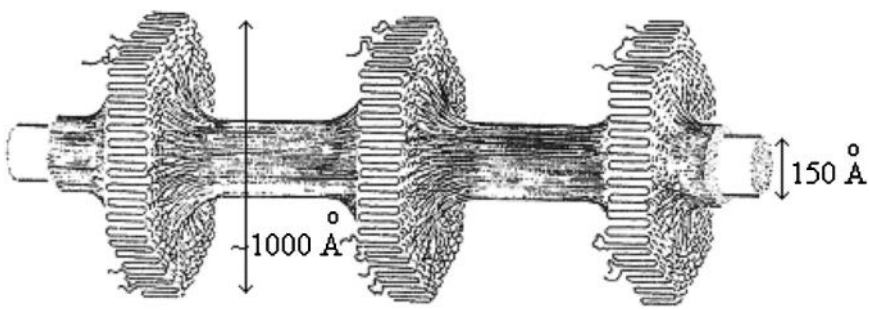

Figure 5.12 Schematic of a section through a shish-kebab structure showing extended core with radial lamellar growth.[30]

orientated microfibrils. These microfibrils are sandwiches of alternating sequences of amorphous and crystalline regions. A great many taut interlamellar tie chains are present and the resulting mechanical properties are excellent. The fibres are formed from stacks of the lamellae and have a very high strength consistent with the crystal structure of the polymer. At high draw ratios the fibres part and significant void structure can be observed between the fibres.

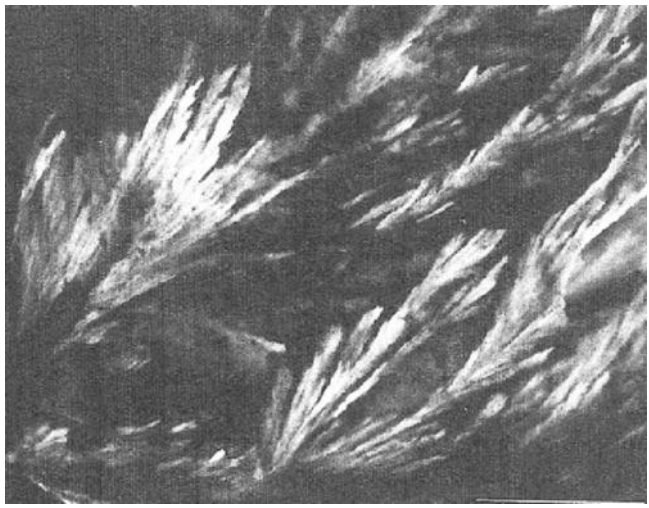

Figure 5.13 Thin film of polypropylene, part of spherulite crossed polars.[31]

Recent studies of highly linear metallocene-synthesized polyethylene of low molecular weight have shown the sheaf-like morphology found in solution is prevalent in the melt phase. The highly linear regular polymers are able very effectively to grow lamellae. The growth of typical lamellae is nicely illustrated in the optical microscopy of Saville[31] (Figure 5.13).

If growth occurs in contact with a nucleating surface then *trans*-crystalline structure is observed. The nucleating object will normally have a flat surface or a fibril. These surfaces become covered with a high density of nucleations resulting in a one-dimensional (columnar) growth in a direction parallel to the normal of the surface. The thickness of the *trans*-crystalline layers depends on the balance between surface nucleation and 'bulk' nucleation.

5.6 Annealing Phenomena

Annealing of monolayer solution-grown single crystals at high temperature leads to crystal thickening and formation of cylindrical holes in the crystals. This 'Swiss cheese' structure of annealed monolayer single crystals is thermodynamically more stable than the original 'continuous' single crystals. This is because the specific surface energy of the hole surface ($\sim$15 mJ m^{-2}) is much less then the specific surface energy of the fold surface ($\sim$90 mJ m^{-2}). Holes do not develop on annealing of mats of overlapping single crystals or melt-crystallized samples.

Polyethylene crystals are observed to thicken at temperatures greater than 110 °C, and if grown under isothermal conditions show this thickening

gradually with time. This thickening process can have a profound effect on the data obtained from scanning differential calorimetry (DSC) measurements. On heating the sample an endotherm is observed associated with the melting process. Observation of the melting temperature as a function of the applied heating rate indicates that the melting point of the crystal is dependent on the heating rate used. Thin crystals have a tendency to thicken as the temperature is raised, prior to melting. The melting temperature decreases with increasing heating rate until finally a constant melting point is attained at the highest heating rate. In Chapter 4 the ability of eicosane chains to move led to the observation of a plastic phase just below the melt temperature. The thickening of the lamellar structure must involve a similar type of motion that allows movement of the folds and an increase in the length of the linear all-*trans* content of the crystal.

It appears that the thickening process occurs in abrupt and discontinuous steps,[32] crystals doubling or trebling their thickness in discrete steps. In melt-crystallized samples with a broad crystal thickness distribution this 'integer' crystal thickness change is not as clearly observed. Experiments on melt-crystallized samples commonly show a linear increase in the average thickness with the logarithm of annealing time. Polyethylene and a few other polymers form extraordinarily thick (micrometres) crystal lamellae after crystallization at elevated pressure, typically at 4–6 kbar. The polyethylene is transformed into a hexagonal phase with appreciable axial disorder at these elevated pressures consistent with the formation of a pseudo-plastic phase. The longitudinal mobility of the chains in such crystals is extremely high in the hexagonal phase as opposed to that of the conventional orthorhombic phase and linear elements of the chain in the lamellae grow past the length of the folded molecules.

Polyethylene has to a large extent dominated morphological studies in polymer systems; however, it is a good model for other systems. Optical microscopy of acetal shows the same characteristic patterns found in polyethylene when a spherulite is viewed under cross-polar imaging (Figure 5.14).

5.7 Experimental Techniques for the Study of Polymer Crystals

Whilst it is not appropriate to discuss the detail of the methods used it is appropriate to mention the principal methods that can be used. More detail of the methods can be found elsewhere.[33,34] The main techniques used are X-ray diffraction for determination of the lattice structure and scanning transmission electron microscopy together with optical microscopy for visualization of the structure. Figure 5.3 was obtained by placing a single crystal on a carbon-coated metal grid and then shadowed with a heavy metal such as gold and viewed using the bright field technique.

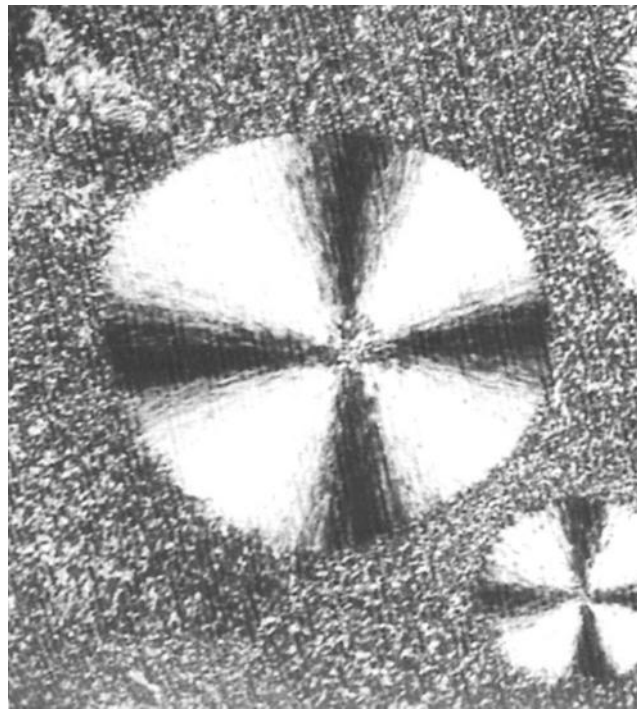

Figure 5.14 Section of acetal (crossed polars).[31]

5.7.1 Optical Microscopy

Polarized light microscopy is the most widely used method for characterizing the morphology of semi-crystalline polymers. Small variations in the local chain orientation produce variations of typically 0.01 or less in the birefringence. Using linear polarized incoming light and a crossed polarizer positioned after the objective lens allows the small differences in birefringence to be used to reveal the morphology. Crystals with their main axis at 45° to the polarizer/analyser pair will transmit the maximum of light; those with their axis parallel to the polarizer will transmit the minimum.

A spherullite is usually pictured as an array of lamellae radially disposed to one another and as a result is 'spherically' birefringent. A spherullite has two unique refractive indices: the radial (n_r) and the tangential (n_t). The refractive index ellipse can represent the variation in refractive index in the plane, where the length of the major axis of the ellipse is proportional to the maximum refractive index in the plane and the length of the minor axis is proportional to the minimum refractive index. If the larger refractive index is in the tangential direction, *i.e.* $n_r < n_t$, the spherulite is termed negative. Spherulites show a characteristic Maltese cross pattern with a maximum in the intensity in the direction at 45° to the polarizer/analyser pair.

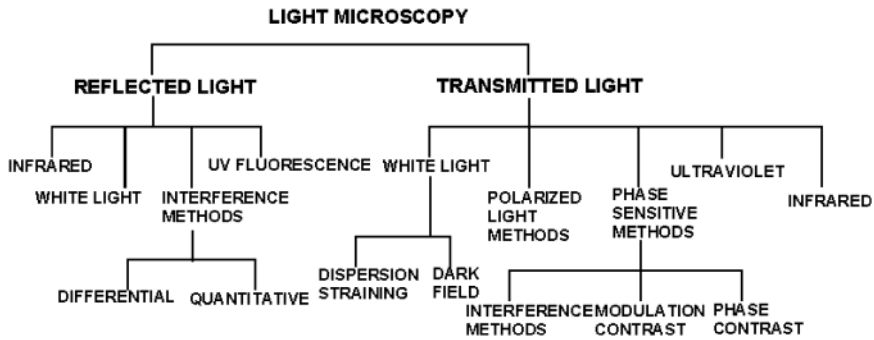

Figure 5.15 Summary of the various types of optical microscopy.

With dimensions on the micrometre scale it is possible for these features to scatter light. For this reason many crystalline polymers are opaque to the human eye. Small-angle light scattering (SALS) can be used to examine pseudo-crystalline material.[33] Using the birefringent nature of the material, studies are used with either H_v (crossed polarizers) or V_v (parallel polarizers). The scattering pattern is recorded, and from the scattering angle (θ_{max}) the average dimensions of the spherulite (R) are determined:

$$R = \frac{4.1\lambda_0}{4\pi n}\left[\sin\left(\frac{\theta_{max}}{2}\right)\right]^{-1} \tag{5.1}$$

where λ_0 is the wavelength of light *in vacuo* and n is the average refractive index of the polymer sample.

This scale of the dimension can be accessed by optical microscopy (Figure 5.15).

The structures themselves are often made up of orientated and organized substructures, as discussed above. The organization within the substructures can be used to aid their visualization. In addition to using direct observation of the specimen, it is possible to obtain images using reflected light. As indicated in Figure 5.15, the techniques that are available can be divided according to whether they are viewed using transmitted or reflected light. The transmitted light techniques require that the samples be obtained in the form of a thin section and require the use of microtome techniques to create these sections.

5.7.2 Microtomes[35]

For polymer work the best and most reliable microtome, in terms of consistently good results, is the base sledge type. Sections will be cut as thin as 0.5 μm, provided the samples are sufficiently rigid. The runners or glides on which the vice, which forms the moving element of the microtome, must also be rigid. The knife blade itself requires a precise edge and may be formed from a diamond edge. For soft samples, it may be necessary to cool the sample and cold working

microtomes are available which can operate at liquid nitrogen temperatures. Alternatively, soft samples can be placed in a rigid resin and then microtomed at room temperature. It is important when carrying out any examination of a polymeric material to observe certain basic rules:

- Handle the sample as little as necessary and use forceps where possible.
- Define the problem and identify which part of the sample requires examination.
- Identify the problem associated with obtaining the specimen in the correct form. Clearly obtaining a thin section can introduce damage that could be misinterpreted as morphology unless it is correctly recognized.
- Assess the size of possible structural features to be examined and areas over which this size might reasonably be expected to vary. It may be necessary to cut 'sighting' section as an aid to making this assessment.

In order to increase the contrast in light microscopy, staining with selective dye molecules that absorb light or have a different refractive index is often used. This process is not widely used in the synthetic polymer field, but there are three specific instances that are worth noting:

- Unsaturated rubbers in sections can be selectively stained black with osmium tetroxide.
- The addition of a fluorochrome to methyl methacrylate used for embedding purposes can be useful in demonstrating impregnation of the specimen.
- Voiding or porosity exposed in cut surfaces can be more easily seen and the extent of penetration established if the surface is impregnated with drawing ink. The technique is to deposit the ink on the surface, subject it to a vacuum cycling routine and then draw off the excess ink with a pipette or tissue. When the remaining ink is dry the surface is polished gently on dry tissue or cloth after which the ink-filled voids will be clearly visible.

Good specimen preparation is the essential precursor of good microscopy. Because of the variability of polymeric materials, not just between types and grades but also between batches, and also the vagaries of processing techniques, each sample will be different from the next. Consequently there are no 'standard routines' or 'magic buttons' that will ensure good results. The secret of success is knowledge of what structural feature requires definition, an appreciation of how the sample will react to different procedures, an awareness and skill to perform as many varied preparation techniques as possible and to modify these as necessary, and patience.

5.7.3 Basic Light Microscopy[36–40]

The simplest approach to light microscopy is the use of a simple configuration in which light is passed through the sample and observed by direct observation of the image. The microscope will usually have a condenser system to focus the

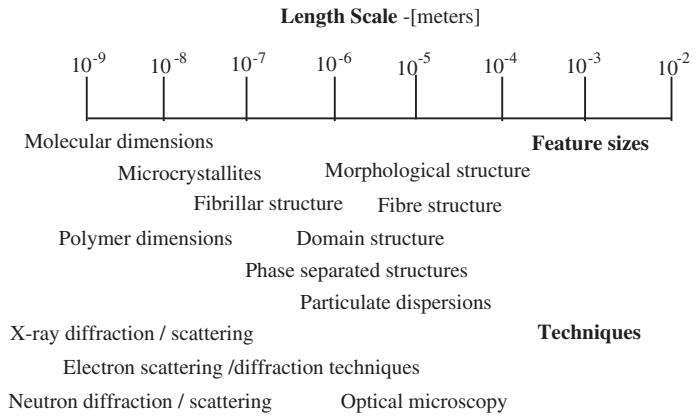

Figure 5.16 The length scale of the feature of interest dictates the appropriate technique for its study.

light into a narrow beam before it passes through the sample. The image is produced by an objective lens system which consists of a number of elements that act together to achieve the desired level of magnification. The observation of an object depends on detection of differences in refractive index between the object and its surroundings. If, as is often the case, the refractive index of the material is fairly uniform across the sample then the specimen may appear to be a uniform bright field. For a feature to be visible there has to be a significant difference in the refractive index of the object relative to the surrounding material.

The scale of the feature that is of interest dictates the preferred technique for its observation (Figure 5.16). Routine light microscopy of plastics and rubber seldom requires the microscope to be used at it limit of resolution.

Indeed, an especially low power $\times 1$ objective lens may be more value in the objective set than a $\times 100$ lens. If the use of higher magnification is necessary it is particularly important with polymeric specimens that the user commences the observation at low power and work up. The interrelationship between microstructural features in polymers can be complex and isolated observations at high magnification can be misleading.

5.7.4 Light versus Electron Microscopy

The microscopic examination of a specimen is usually embarked upon with a clear aim in mind. It is the problem that should dictate the choice of method and the examination will often justify the use of a range of microscopy techniques.

In very general terms, light microscopes are cheaper than their electron counterparts, less expensive to run and there are almost no problems of adverse interactions between the specimen and the radiation used. In the light

microscope, the specimen is not exposed to vacuum and the specimen preparation procedures are fairly straightforward and flexible.

The great advantages offered by the electron microscope are substantially higher resolution in several modes of operation and, through accessories, elemental analysis of very small volumes. An increased depth of field is another advantage, at least in the case of conventional scanning microscopy. This allows easier image interpretation and a more precise understanding of the spatial interrelationship of features in the image. The disadvantages in relation to electron microscopy are electron beam damage and the use of high vacuum. A chapter later in this volume will consider the use of environmental scanning electron microscopy, when these problems are to some extent addressed.

5.7.5 Phase Contrast Microscopy

If a grating is inserted in the microscope it is possible to create diffraction effects in the back focal plane of the objective lens. The creation of a phase difference between the diffracted and undiffracted light can often increase image visibility. Specifically the aim is to increase the phase difference from around 90° to 180°. This can be accomplished by allowing the undiffracted light to pass through a thin plate (a 'phase' plate) of such a thickness that placing the plate in the back focal plane of the objective produces the necessary phase shift. At this point, the zero-order diffracted light can be located in a separate plane from the diffracted light, but to do this it is necessary to restrict the illumination cone from the condenser lens. The process of restriction of the cone of light by closing down the aperture iris gives a collimated beam. The zero-order diffraction maximum would then be clearly located at the centre of the back focal plane of the objective.

In practice, phase contrast systems may be 'positive' or 'negative'. For the former, higher refractive indices in the specimen will appear as being darker than the surrounding field; in negative phase contrast the situation is reversed. However, the contrast actually seen will also depend on the magnitude of the phase shift (or optical path differences) in the specimen. Examination of thin films of polymers may reveal knife marks since the knife creates regions of differing thickness and this will introduce phase shifts. In phase contrast, microscopy knife marks may be made substantially more visible than with straight transmission techniques.

5.7.6 Polarized Light Microscopy[40]

Additional information can be obtained on many polymeric materials by use of polarized rather ordinary white light. When a beam of unpolarized light is directed on a crystal of a material (such as calcite), it is found that there are two refracted beams instead of the usual one. This effect can lead to a duplication of the image, when examining an object through calcite crystal. These two beams can be shown to be polarized at right angles to one another by viewing the image through a sheet of polaroid. As the polaroid is rotated, first one image

will be extinguished so that only one image remains, and on rotation through a further 90° the other image will disappear. The light can be described as being elliptically polarized, indicating that it consists of two components vibrating at right angles to one another. This concept and notation finds greatest use in situations where polarized light traverses more than one thin plate, in which case analysis by resolution of the beam into its individual components becomes quite complex.

5.7.7 Origins of Birefringence

Organized structures are often able to induce optical birefringence and when viewed using polarized light will have enhanced contrast. Imaging using crossed-polarizers or with the aid of birefringent fluids can assist with the visualization of the order within the structure. The substructure can usually be revealed by the selective use of solvent systems that will allow differential swelling of the sample, use of dyes which are selective for a particular type of chemistry or through the use of the structures themselves as revealed through the use of polarized light. In a polymer such as cellulose, it is possible to identify regions of high order within a fibre surrounded by areas of the reverse order or high disorder, and follow the changes that occur during the processing of the fibres.

5.7.8 Orientation Birefringence

In a system such as cellulose, addition of dibutylphthalate to the fibres will reveal the sub-micrometre order through changes in the birefringence of the fibres.[34] The magnitude of the birefringence can also provide information on the nature of the chain packing and the orientation of the molecules that produce the polarization changes. Orientation birefringence is produced by the alignment of molecules that are themselves optically anistropic, as is generally the case for polymer chains. Polymer chains can be considered to have a different refractive index parallel to the chain direction from that perpendicular to it. When the chains are randomly arranged as in the melt or in amorphous materials then the net refractive index is intermediate between the two separate values. When either crystallization or alignment due to drawing aligns the polymer chains then differences in the refractive index arise and birefringence can be detected. Many polymers are subjected to a drawing process during their fabrication, as in the manufacture of fibres and films, or as a by-product of the deformation that occurs in many processes such as compression or injection moulding. Measurement of the birefringence can in principle be used to indicate the extent to which orientation is being induced in that material.

5.7.9 Strain Birefringence[38]

Application of strain to a material or the presence of residual stress remaining from the production process can generate orientation that is detected as

birefringence. The superimposed stress can alter the distance between atoms of the material, thus changing the polarizability of the bonds in the direction of the applied stress and hence creating a difference in refractive index in the material between the stress direction and directions perpendicular to it. This effect can occur equally well with molecules that are optically isotropic in the unstrained state and those that are naturally anistropic.

5.7.10 Form Birefringence[38]

Form birefringence is found in materials that have two or more phases with different refractive indices. A number of polymers are able to undergo phase separation and create on a nano-dimensional scale regions of homogeneity but distinctly different dielectric properties. If one phase is in the shape of rods or plates with smallest dimensions less than the wavelength of light, the refractive index of the whole material parallel to the rods is different from that perpendicular to the rods, even when both phases are themselves isotropic. Effects of this type are found in styrene–butadiene–styrene block copolymers.[34] It is possible in some cases to estimate the contribution of form effects to the total birefringence by selectively swelling one of the phases in various liquids of different refractive index. The form birefringence will in theory fall to zero when the refractive index difference between the phases is reduced to zero.

5.7.11 Polarization Colours[38]

When a wedge of material is viewed using monochromatic light a series of regularly spaced dark bands can sometimes be observed corresponding to points where the product of the thickness and the birefringence is a whole number of wavelengths. However, white light, which is more usually used to examine specimens, contains a continuous spread of wavelengths between about 400 nm and 750 nm, so destructive interference will occur at a different path difference for each part of the spectrum. Therefore, at no point can there be total darkness, for a specimen viewed in white light. For a specimen with a given (non-zero) optical path difference there will be subtraction from the incident white light of that wavelength for which the path difference is an integral multiple. Other wavelengths will also be reduced in intensity to a decreasing extent the further they are removed from this particular wavelength. With thicker or more birefringent specimens the path difference can be a multiple of more than one wavelength at the same time. The resulting complex subtraction of wavelengths from the incident white light produces a characteristic colour that can be related by use of a chart to the optical path difference producing it. Thus identification is only possible at the lower end of the path difference scale. The refractive index differences and birefringence can in principle be measured using references such as the quartz wedge or the Babinet compensator.

5.7.12 Modulation Contrast Techniques[39]

It is desirable to attempt to enhance the contrast of an object to be imaged. A modulation contrast system (MCS) and differential interference contrast (DIC) system can significantly help in this respect. The MCS and DIC systems detect the optical gradients and convert them to intensity variations. Since the eye can only detect colour and intensity variation detail in non-absorbing (phase) objects, a piece of transparent polymer is normally invisible. The optical gradient occurs at the curved or sloped portion of an object and is the rate of change in optical path difference between the object and its surroundings. A changing gradient can in effect act as a prism and would lead to refraction. In the very local region of the edge of the object there will be a refractive index gradient that in principle should allow visualization of the object. However, if the edge is not sharp then the gradient is small and visualization will be difficult. The factors that influence the ability to see the object are its size, edges and curvature of the object. The quality of the image will in turn depend on the wavelength of light, the diffraction process and the relative coherence of the light just prior to its interaction with the object. Since the mid wavelength in the visible spectrum is about 0.5 μm, physical features around this size create strong diffraction effects. The image of these features depends on the recombination (interference) of the diffracted waves at the image plane. The visibility of this interference process is dependent on the relative coherence of light at the moment of interaction with the object. The greater the coherence the greater the visibility of the interference process and thus the more visible are the images of the diffraction sites in the object. In a microscope the aperture of the condenser system controls the coherence of the light that reaches the object plane. As the condenser aperture is decreased it is usually observed that the visibility of the edges and particles of an object may be increased, although the resolution is reduced.

In the MCS, an additional slit is added with a polarizer as part of the condenser lens system. The modulation contrast microscope is best discussed in terms of the object being imaged as a small prism. Light passes through the object (prism) and then through the objective. The light coming from the object is then examined using a special filter. The filter has three elements representing different degrees of attenuation of the light from the object. Diffracted light passing through the unattenuated region of the filter is combined with light that is attenuated by about 15% of its original intensity. The intensity of the image is controlled by the transmission factor of that portion of the modulator thorough that the light passes. After passing through the modulator the light forms a bright image of the prism at the real image plane. The overall result is that combination of the shifted and non-shifted waves leads to enhanced contrast and greater visibility of the object. The enhanced clarity that is possible without loss of resolution has enabled fine features associated with local stress concentrations, *etc*., to be imaged in otherwise transparent materials.

5.7.13 Interference Microscopy[40]

If two waves of light are out of phase then they are capable of producing constructive and destructive interference. Although two waves may have identical wavelengths and amplitudes, if one lags behind the other along the time axis then they will be 'out of phase' and a change in amplitude will result in the combined wave. One of the simplest methods to create an interference situation is to use flat cover slips that are coated with a thin semi-reflecting layer of metal such as gold or aluminium. The thickness of the coating is not particularly critical but should be thin enough to allow approximately 50% of the light to be transmitted. The phase delay is introduced between the reflected and transmitted waves and the cover slips form the basis of a conventional interferometer structure. Closing down the aperture iris increases the visibility of the interference fringes but can restrict the lateral resolution by increasing fringe contrast. The fringes observed can be interpreted as variations in the path length through the sample and associated with thickness variations in morphological features or, in the case of observation of a surface, variation in roughness.

5.8 Electron Microscopy

Perhaps the most common method for the study of morphology is electron beam microscopy. For very thin samples it is possible to use transmission methods and in principle the elastically scattered electron image can be used to determine the lattice dimensions. To enhance the contrast and aid the image definition the sample will typically be coated with a layer of gold or conducting carbon. This process minimizes the charge build-up on the surface and in the case of gold shadowing enhances the scattering and makes features more visible.[34,35] For both optical and electron beam microscopy etching of the sample can help reveal the detail of the molecular organization which exists.

5.8.1 Sample Preparation: Etching and Staining

For solution-grown very thin crystals direct examination is possible. However, for bulk materials either thin sections have to be created with the use of a low-temperature microtome or internal surfaces can be exposed through fracture of the material. In both cases the process of sample preparation can induce damage and great care has to be taken that the features identified are not artefacts of the sample preparation method. To enhance the contrast it is sometimes appropriate to etch the material.

The mildest form of treatment involves solvent etching, which relies on low melting point being more easily dissolved than the bulk of the material. In crystalline materials phase segregation can occur and hence this process can be very useful in outlining spherulite boundary layers and similar vulnerable areas.

The solvent can be used as part of a polishing process and the creation of smooth surfaces reveals more clearly the underlying morphological features.

There are essentially two main etching techniques: vapour etching for only a few seconds; and controlled isothermal treatment with a liquid solvent for a considerably longer time (several hours). A solvent etching temperature (T_d) is selected on the basis of the melting point of the segregated species (T_m):

$$T_d = T_m - \Delta T \tag{5.2}$$

where ΔT is dependent on the solvent power. For etching polyethylene with *p*-xylene, ΔT is 31 K.

For optical and electron microscopy etching and selective degradation of material can be helpful. Various approaches are used. Plasma etching will create oxygen-containing functions as will etching with permanganic acid. Other favoured etchant systems include etching with chlorosulfonic acid and staining with uranyl acetate. Sulfur, chlorine, oxygen and uranium add selectively to the amorphous component. Unsaturated polymers like polybutadiene or polyisoprene can be stained with OsO_4 that adds selectively to the double bonds located in the amorphous phase. Ruthenium tetraoxide (RuO_4) has proven useful for preparing samples with other types of double bond, e.g. polystyrene and polyamides.

In the case of electron beam microscopy optimum contrast is obtained when the fold surface is parallel to the electron beam. Tilted crystals appear less sharp and areas without lamellar contrast are found over large areas of the electron micrographs. This is one of the disadvantages of these methods. Only a small fraction of the crystals can be viewed at the same time. The use of a tilting stage permits the assessment of more lamellae, *i.e.* lamellae of other tilt angles are included in the analysis. Another problem is shrinkage of the whole section that may occur in the sample due to dissipation of the electron beam energy. Samples etched with chlorosulfonic acid for only a short period of time showed significant shrinkage, whereas samples treated with acid for a long period of time showed only negligible shrinkage.

An alternative method is to use mixtures of concentrated sulfuric acid and potassium permanganate, giving contrast between crystals and amorphous domain that turns out to be applicable to many different polymers, e.g. polyethylene, polypropylene, poly(but-1-ene), polystyrene and poly(aryl ether ketone)s. The strong etchant degrades the amorphous phase more quickly than the crystals and the resulting topography is revealed by heavy metal shadowing. Replicates are prepared which are examined in the electron microscope.

5.9 X-Ray Diffraction[34]

X-Ray diffraction is used to provide information on the lattice dimensions but can also provide so-called long period data. The long period is the sum of the amorphous and the crystalline lamellae dimensions and is studied using

small-angle X-ray scattering (SAXS). The periodic variation in the electron density along a line perpendicular to the fold planes gives rise to constructive interference at a very small scattering angle. The average crystal thickness (L_c) is given by

$$L_c = dv_c \tag{5.3}$$

where v_c is the volume fraction of the crystalline component and d is the SAXS long period. Wide-angle X-ray diffraction is used to determine the crystal size through the use of the Scherrer equation:

$$\overline{D_{hkl}} = \frac{K\lambda}{\beta \cos\theta} \tag{5.4}$$

where K is the Scherrer shape factor, which adopts values close to unity, λ is the wavelength of the X-rays and β is the breadth in radians at half the peak height of the diffraction peak associated with the $\{hkl\}$ planes, where $\overline{D_{hkl}}$ is the crystal thickness. This expression assumes that the main cause of broadening is the distribution of the crystal orientations but thermal vibrations and paracrystalline distortions can also contribute. These effects are accommodated in the following equation:

$$\beta_s^2 = \frac{1}{\overline{D_{hkl}^2}} + \frac{\pi^2 g^4}{d_0^2} n^4 \tag{5.5}$$

where β_s is the breadth of the diffraction peak in scattering units ($s = (2\sin\theta)/\lambda$) after subtracting the instrumental broadening contribution, d_0 is the interplanar distance for the first-order reflection, n is the order of reflection and g is the degree of statistical fluctuation of the paracrystalline distortions relative to the separation distance of the adjacent lattice cell. If β_s^2 is plotted as a function of n^4 the thickness $\overline{D_{hkl}}$ is obtained as the square root of the reciprocal of the intercept. More details can be found elsewhere.[34]

5.10 Raman Scattering and Phonon Spectra[35]

The crystal thickness in polyethylene has been determined using Raman spectroscopy by measurement of the frequency of the longitudinal acoustic mode (which is inversely proportional to the length of the all-*trans* stems in the crystals) and size exclusion chromatography of samples etched with HNO_3 or O_3. Both the acid and ozone degrade the amorphous parts and leave essentially oligomers with chain lengths equal to the all-*trans* length ($L_c/\cos\theta$, where θ is the tilt angle).

5.11 Degree of Crystallinity[34]

Because of the complex manner in which the lamellae grow and interact, the crystalline content of bulk samples can vary significantly. Determination of the degree of crystallinity is a very useful indicator of the morphology of the

material. For simplicity it is assumed that the bulk material exists either as a crystalline or an amorphous phase and that any intensive property (ϕ) is an additive function with contributions from the two components present:

$$\phi = \phi_c w_c + \phi_a(1 - w_c) \tag{5.6}$$

where ϕ_a and ϕ_c are, respectively, properties of the crystallinity of the amorphous and crystalline phases and w_c is the mass of the crystalline phase. This equation can be applied with intensive properties such as the enthalpy, specific heat or specific volume of the material.

5.11.1 Density and Calorimetric Methods

The most obvious difference between amorphous and crystalline regions is the density of chain packing. Accurate measurements of the density, with a precision of about 0.2 kg m^{-1}, are carried out in a density gradient column or alternatively by a floating method, and then very accurate measurement of the mixture density. The mass crystallinity can be obtained from the following equation:

$$\frac{1}{\rho} = \frac{w_c}{\rho_c} + \frac{(1 - w_c)}{\rho_a} \tag{5.7}$$

where ρ, ρ_c and ρ_a are, respectively, the densities of the sample, crystalline component and amorphous component. The density of the crystalline component is usually determined from the X-ray unit cell data and the amorphous density is obtained by extrapolation of dilatometric data of molten polymer to lower temperatures. The principal problem with the density measurement is the possibility of the liquids used swelling the samples. It is usually possible by the correct selection of solvent system to minimize this problem.

The ready availability of differential scanning calorimetry (DSC) and in recent years moduluated DSC have significantly increased the use of the enthalpy of fusion of crystals as a method for crystallinity determination. An illustration of this method was shown for plastic crystals in Chapter 4. The enthalpy of the solid is a combination of components from the amorphous H_a and crystalline H_c regions. The enthalpy at any given temperature H is therefore

$$H = H_c w_c + H_a(1 - w_c) \tag{5.8}$$

where w_c is the mass crystallinity. In practice, annealing processes will influence the distribution between crystalline and amorphous regions making determination of the value of w_c problematic. If, however, the internal stresses are negligible and it is assumed that the amorphous component is liquid-like, *i.e.* the amorphous phase enthalpy at $T < T_m$ can be obtained by extrapolation of data from temperatures greater than T_m, then enthalpy (H_1) at a temperature T_1 well below the melting temperature range is

$$H_1 = H_{c1} w_{c1} + H_{a1}(1 - w_{c1}) \tag{5.9}$$

where w_{c1} is the crystallinity at T_1 and H_{c1} and H_{a1} are the crystalline and amorphous enthalpies, respectively, at T_1.

At T_2 ($\gg T_m$) the enthalpy is given by

$$H_2 = H_{a2} \tag{5.10}$$

The difference in enthalpy of the sample between temperatures T_1 and T_2 is given by

$$\Delta H_{21} = H_2 - H_1 = [H_{a2} - H_{a1}] + [H_{a1} - H_{c1}]w_{c1} = \Delta H_{a21} + \Delta H^0_{f_1} w_{c1} \tag{5.11}$$

That is,

$$w_{c1} = \frac{\Delta H_{21} - H_{a21}}{\Delta H^0_{f_1}} \tag{5.12}$$

where $\Delta H^0_{f_1} = H_{a1} - H_{c1}$ is the heat of fusion at T_1 and $\Delta H^0_{f_1}$ is temperature dependent:

$$\Delta H^0_{f_1} = \Delta H^0_{T^0_m} - \int_{T_1}^{T^0_m} [C_{pa} - C_{pc}]\, dt \tag{5.13}$$

where C_{pa} and C_{pc} are, respectively, the specific heats at constant pressure of the amorphous and crystalline components.

In order to determine $\Delta H_{21} - \Delta H_{a21}$, it is necessary to extrapolate the post-melting scanning baseline down to lower temperatures. Often the extrapolated baseline intersects the premelting scanning baseline and this helps selection of T_1. The area under the curve starts at T_1 and ends once melting has been completed. More details on the methods can be obtained elsewhere.[34]

5.11.2 X-Ray Scattering

The most direct method of determining the degree of crystallinity is X-ray scattering. The intensity of the structural lines (coherent scattering) in the total scattering spectrum arises from the unit cell and other ordered features. Thus the ratio of the coherent scattering to the total scattering is directly related to the crystalline fraction. The amorphous component will add a broad background to the scattering spectrum. Thus the total coherent scattering from N atoms is independent of the state of aggregation and the mass crystallinity can be defined as

$$w_c = \frac{\int_0^\infty s^2 I_c(s)\, ds}{\int_0^\infty s^2 I(s)\, ds} \tag{5.14}$$

where I is the total scattered intensity which contains amorphous and crystalline components and I_c is the scattered intensity associated with the crystalline regions and corresponds to the Bragg reflections. In eqn (5.14), s is the scattering parameter which is equal to $(2\sin\theta)/\lambda$, where λ is the wavelength.

The practical problems encountered in determining w_c arise from three principal sources. Often the coherent Bragg peaks are superimposed on a broad incoherent scattering peak and some form of subtraction has to be applied to separate the contributions. The denominator should contain the total scattering from all sources; however, it is sometimes difficult to have a sufficiently wide range of angles to be sure that all the contributions from incoherent scattering are included. As indicated above, the coherent scattering will also contain components from thermal vibrations and paracrystalline defects that are difficult to allow for in the estimation of the coherent scattering intensity. Various approaches have been developed but all have limitations.

5.11.3 General Observations

Usually X-ray and density data are in good agreement. The degree of crystallinity for most polymers will depend on the ability of the chains to pack regularly together. Disruption of the structure will introduce defects that will reduce the crystallinity. Ethyl branches on a linear polyethylene backbone can cause reduction in the degree of crystallinity to the extent of 20% per mol% of ethyl groups.[41] The ethyl groups are probably located in the fold and hence segregated where possible to the amorphous phase. Polymers with larger branches, propyl or longer homologues, are fully non-crystallizable unless the branch becomes of sufficient molar mass to look like a short polymer. The molar crystallinity depression of smaller groups, carbonyl and methyl groups, is less than that due to ethyl groups.

In general, the crystallinity increases with increasing molar mass. Very low molar mass polymers crystallize in extended chains or once- or twice-folded crystals and form almost perfect crystals. Increasing the molar mass of the polymer increases the possibility of chains leaving one lamella and entering another, with a consequent disruption of the perfect order. Chain entanglements play an important role controlling the extent to which various parts of the chain can be incorporated in particular lamellae. The effect of the entanglements can be to suppress the crystallinity so that for a linear polyethylene of $\bar{M}_w = 106\,\mathrm{g\,mol^{-1}}$ the crystallinity is between 40 and 50%.

5.12 Conclusions

Although the structures that are observed with electron microscopy look complex, it is apparent that they are all related to the chain folded lamellae to a lesser or greater extent. Defects in the lamellar structure, as with simple organic crystals, will control the habit of the crystals form. The spherulitic

structures observed are a consequence of the multiple growth of lamellar structures and their tendency to splay with growth. Naturally occurring polymer materials exhibit more complex morphology and this topic will be briefly considered later in this book. It is now appropriate to consider the factors that influence the growth of these lamellar structures.

Recommended Reading

D.C. Bassett, *Principles of Polymer Morphology*, Cambridge University Press, Cambridge, 1981.
D. Campbell, R.A. Pethrick and J.R. White, *Polymer Characterization*, Stanley Thornes, Cheltenham, UK, 2000.
U.F. Gedde, *Polymer Physics*, Chapman & Hall, London, 1995, ch. 7.
H. Hasegawa and T. Hashimoto, in *Comprehensive Polymer Science Second Supplement*, ed. G. Allan, Pergamon, Oxford, 1996, p. 497.
D.A. Hemsley (ed.), *Applied Polymer Light Microscopy*, Elsevier Applied Science, London, 1989.
M. Srinivasarao, in *Comprehensive Polymer Science Second Supplement*, ed. G. Allan, Pergamon, Oxford, 1996, p. 163.
S. Vaughan and D.C. Bassett, in *Comprehensive Polymer Science*, ed. G. Allan and J.C. Bevington, Pergamon, Oxford, 1989, vol. 2, p. 415.

References

1. U.F. Gedde, *Polymer Physics*, Chapman & Hall, London, 1995, ch. 7.
2. S. Brückner and S.V. Meille, *Nature*, 1989, **340**, 455.
3. G. Natta and P. Corradini, *Novovo Cimento Suppl.*, 1960, **15**, 40.
4. J.L. Koenig and A.C. Angood, *J. Polym. Sci., Part A2*, 1970, **8**, 1787.
5. T. Miyazawa, K. Fumushima and Y. Iideguchi, *J. Chem. Phys.*, 1962, **37**, 2764.
6. T. Miyazawa, *J. Chem. Phys.*, 1961, **35**, 693.
7. H. Tadokoro, in *Molecular Structure and Properties*, Physical Chemistry Series 1, ed. A. D. Buckingham and G. Allan, Butterworths, London, 1972, vol. 2, p. 45.
8. A. Keller, *Philos. Mag.*, 1957, **2**, 1171.
9. P.H. Till, *J. Polym. Sci.*, 1957, **24**, 30.
10. E.W. Fischer, *Z. Naturforsch.*, 1957, **12a**, 753.
11. A.S. Vaughan and D.C. Bassett, in *Comprehensive Polymer Science*, ed. G.Allan and J.C. Bevington, Pergamon, Oxford, 1989, vol. 2, p. 415.
12. L. Mandlekern, *Physical Properties of Polymers*, American Chemical Society, Washington, DC, 1984, ch. 4.
13. (*a*) D.C. Bassett, *Principles of Polymer Morphology*, Cambridge University Press, Cambridge, 1981; (*b*) K.H. Storks, *J. Am. Chem. Soc.*, 1939, **60**, 1753.

14. T. Kawai and A. Keller, *Philos. Mag*., 1985, **11**, 1165.
15. A. Peterlin, in *Structure and Properties of Orientated Polymers*, ed. I. M. Ward, Wiley, Chichester, 1975, ch. 2, p. 36.
16. S.J. Organ and A. Keller, *J. Mater. Sci*., 1985, **20**, 1571.
17. H.D. Keith and F.J. Padden, *J. Appl. Phys*., 1964, **35**, 1270.
18. D.C. Bassett and A. Keller, *Philos. Mag*., 1962, **7**, 1553.
19. F. Khoury and F.J. Padden, *J. Polym. Sci*., 1960, **47**, 455.
20. D.C. Basset, *Morphology Encyclopaedia of Polymer Science and Technology*, John Wiley, New York, 2003.
21. D.C. Basset, *Philos. Mag*., 1964, **10**, 595.
22. D.C. Basset, *Philos. Mag*., 1965, **12**, 907.
23. A.M. Hodge and D.C. Bassett, *J. Mater. Sci*., 1957, **12**, 2065.
24. M.I. Abo and D.C. Bassett, *J. Macromol. Sci. Phys*., 2001, **B40**, 849.
25. M.I. Abo and D.C. Bassett, *Polymer*, 2001, **42**, 4957.
26. A. Keller, *Kolloid Z. Z. Polym*., 1967, **219**, 118.
27. A.S. Vaughan and D.C. Bassett, in *Comprehensive Polymer Science*, ed. G. Allan, Pergamon, Oxford. 1989, vol. 2. p. 432.
28. D.A. Hemsley, in *Applied Polymer Light Microscopy*, ed. D.A. Hemsley, Elsevair Applied Science, London, 1989, p. 67.
29. P.K. Datta and R.A. Pethrick, *Polymer*, 1978, **19**, 145.
30. A.J. Pennings, *J. Polym. Sci. Polym. Symp*., 1977, **59**, 55.
31. B.P. Saville, in *Applied Polymer Light Microscopy*, ed. D.A. Hemsley, Elsevier Applied Science, London, 1989, pp. 67–112.
32. G. Ungar, J. Stejny, A. Keller, I. Bidd and M.C. Whiting, *Science*, 1985, **229**, 386.
33. R.A. Pethrick and C. Viney, *Techniques for Polymer Organisation and Morphology Characterisation*, John Wiley, Chichester, UK, 2003.
34. D. Campbell, R.A. Pethrick and J.R. White, *Polymer Characterization*, Stanley Thornes, Cheltenham, UK, 2000.
35. A.D. Curson, in *Applied Polymer Light Microscopy*, ed. D.A. Hemsley, Elsevier Applied Science, London, 1989, p. 19.
36. B.P. Saville, in *Applied Polymer Light Microscopy*, ed. D.A. Hemsley, Elsevier Applied Science, London, 1989, p. 73.
37. M.J. Folkes and A. Keller, *Polymer*, 1971, **12**, 222.
38. R. Hoffman, in *Applied Polymer Light Microscopy*, ed. D.A. Hemsley, Elsevier Applied Science, London, 1989, p. 151.
39. D.A. Hemsley, in *Applied Polymer Light Microscopy*, ed. D.A. Hemsley, Elsevier Applied Science, London, 1989, p. 151.
40. P. Calvert and N.C. Billingham, in *Applied Polymer Light Microscopy*, ed. D.A. Hemsley, Elsevier Applied Science, London, 1989, p. 233.
41. T. Tranker, M. Hendenqvist and U.W. Gedde, *Polym. Eng. Sci*., 1994, **34**, 1581.

CHAPTER 6

Polymer Crystal Growth

6.1 Introduction

The processes involved in the formation of a crystalline polymeric solid are complex and still open to some debate. Using the analogy of the short-chain hydrocarbon dodecane (Chapter 1), the crystallization process simplistically involves the creation of favourable interactions between neighbouring chains. However, such an approach does not recognize the unique features possessed by polymers: restricted chain mobility and the effects of entanglement and other long-range interactions.

6.1.1 Thermodynamics of Polymer Molecule in the Melt

The energy of a polymer molecule in the molten state will be determined by a combination of inter- and intramolecular forces. Within the polymer molecule, the atomic interactions that produce the barriers to internal rotation will also create the energy differences that will define the heat capacity. In Chapter 1, the energy profile for the rotation about a single bond was discussed and it was pointed out that molecules can occupy either the lower energy *trans* or the higher energy *cis* or *gauche* state. The success of the RISM theory[1] was in the prediction of the effects of temperature on the size and shape of the polymer molecule. The RISM predicts that as the temperature is raised the occupancy of the higher energy states is increased so the size of the polymer coil *shrinks*. In the melt state, the polymer molecule will attempt to adopt a minimum coil size and the collapse for higher molecular mass polymers is restricted by the effects of entanglement and so-called 'excluded volume' effects. The excluded volume effect describes the restrictions that have to be placed on the theoretical polymer chain to avoid it occupying the same point in space as another element of either the same chain or of that of another polymer.

Cooling a polymer chain will increase the proportion of the coil which exists in the extended all-*trans* form and this will facilitate the creation of the *stem* structures which are required for crystal growth. The polymer chains are not static entities and changes in the location of the *gauche* conformations can disrupt the formation of favourable interactions for crystal growth, suppress nucleation or alternatively assist the creation of *stems* of the correct length and

aid nucleation. If two or more *gauche* sequences become located close together on the chain a *hair pin* or *folded* structure is generated which aids the growth process. The number of such folds will have an equilibrium value at a particular temperature. Although intuitively one might expect polyethylene chains to adopt an extended regular structure, both solution-grown and melt-grown crystals are chain *folded*. The attachment process may involve either the end of chains or a low-energy all-*trans* section interacting with a preformed surface. The ends of chains will have a higher energy than the central sections and hence ends tend to be located at surfaces. Clearly, the process of attachment of the polymer chain to the surface involves not just a change in enthalpy but also subtle changes in the total entropy of the system. The process of nucleation should ideally only involve interactions between polymer molecules, but in practice residual catalysts and other solids present in the melt help the process.

The concept of chain folding is core to understanding the nature of the crystalline polymeric state and this was first recognized by Keller.[2,3] It is easy to visualize that as the polymer chain is being laid down on the substrate, folding will occur and energetically the process would drive the folds to be located at a surface. As a consequence, the polymer tends to form stacks of extended polymer chains which we ascribe the term *lamellae* and these have a thickness which is indicative of the temperature at which they were grown. This observation is consistent with the polymer chain having a distribution of conformational states and entropy defined by that population. Trapped within the crystalline material will be disordered *amorphous* material that is in a non-equilibrium state.

6.1.2 Nucleation

The nucleation and growth processes, similar to the situation in low molar mass organic crystals, are dependent on the degree of supercooling of the melt or solution phase. The crystal thickness or alternatively the thickness of each new crystalline layer in a growing crystal is the one that grows fastest rather than the one that is at equilibrium. There is a wealth of information available on the crystallization of many polymers as well as several theories that aim to predict the crystallization rates, crystal shapes and lamellar thicknesses.

Once the chain has attached itself to the substrate it is possible that as neighbouring chains start to build subsequent layers of the crystal, the energy balance may change. As a consequence the possibility of the original structure changing to a new more stable structure exists. This leads to the phenomenon of *polymorphism* and is well known in both small organic crystals and in crystalline polymers.

In the melt phase, thermodynamics would indicate that chains with different chain lengths should have different energies. As a consequence there is the possibility that chains with a similar energy will tend to segregate themselves in space. *Phase separation* is well known in polymer blends (Chapter 8) and can be described by the process of spinodal decomposition. In the case of a broad molecular mass distribution polymer system, the individual chains will

fractionate according to their molar mass and the morphology of the crystals can reflect this effect. However, the viscosity of the melt during the crystallization process will usually stop an equilibrium state being achieved and hence phase diagrams often give little insight into the state of the material during the crystallization process.

Whilst it is relatively straightforward to describe the processes involved in polymer crystallization, it is far more difficult to articulate in terms of a model that allows the quantitative prediction of the crystallization process.[4]

In Chapter 5 it was identified that in crystalline polymeric material lamellae constitute a major fraction of the material. In Chapter 2 it was shown that crystal growth depends on the molecule becoming attached to the crystal surface at the lowest energy. In the case of polymer chains, the attachment is of a length, linear *stem*, in the case of polyethylene an all-*trans* structure being attached to a similarly organized set of molecules. As with organic crystals, the *habit* of the crystal that grows depends on the occurrence of defects and the relative growth rate of each of the faces of the lattice involved. The equilibrium shape of a crystal is therefore the result of molecules searching for the minimum energy. High-energy surfaces should be relatively small and the crystal dimensions perpendicular to those surfaces large because the *stems* will be much longer than they are wide with the result that the growth rate is much greater than attachment to the fold surface. It is not very surprising therefore to find that lamellar sheets dominate the discussion of crystal growth in polymer systems.

6.2 Minimum Energy Conditions and Simple Theory of Growth[4–6]

Simplistically, we can consider the relative energy of attachment to a cube with faces 1, 2, 3 (Figure 6.1).

The dimensions of the crystal will be determined by the relative energy of each surface and will be a minimum with respect to the melt (ΔG) at a given volume:

$$\Delta G = V\Delta G_{\mathrm{m}}^{0} + 2L_1L_2\sigma_3 + 2L_1L_3\sigma_2 + 2L_2L_3\sigma_1 \tag{6.1}$$

where $\Delta G_{\mathrm{m}}^{0}$ is the specific free energy of melting and σ_i are the specific surface free energies. This equation is true for any crystal growth process and is not

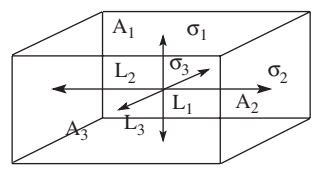

Figure 6.1 Equilibrium shape of a crystal with three different surfaces ($i = 1, 2, 3$) with different surface free energies σ_i.

specific for a polymer system. One of the L_i terms can be eliminated from the equation by considering that $V = L_1L_2L_3$ is constant, thus:

$$L_3 = V/(L_1L_2) \tag{6.2}$$

Inserting eqn (6.2) into eqn (6.1) yields

$$\Delta G = V\Delta G_m^0 + \frac{2V}{L_3}\sigma_3 + 2L_1L_2\sigma_2 + \frac{2V}{L_1}\sigma_1 \tag{6.3}$$

Taking the derivatives of ΔG with respect to L_1 and L_3 and setting each component equal to zero, the following expressions are obtained:

$$\frac{\partial(\Delta G)}{\partial L_1} = L_3 - \frac{V}{L_1^2}\sigma_1 = 0 \Rightarrow \frac{L_1}{\sigma_1} = \frac{L_2}{\sigma_2} \tag{6.4}$$

and

$$\frac{\partial(\Delta G)}{\partial L_3} = L_1\sigma_2 - \frac{V}{L_3^2}\sigma_3 = 0 \Rightarrow \frac{L_2}{\sigma_2} = \frac{L_3}{\sigma_3} \tag{6.5}$$

Combining eqn (6.4) and (6.5) gives

$$\frac{L_1}{\sigma_1} = \frac{L_2}{\sigma_2} = \frac{L_3}{\sigma_3} \tag{6.6}$$

Equation (6.6) indicates that the dimensions of the equilibrium crystal in different directions (i) are proportional to the surface free energies (σ_i) of the perpendicular surfaces. This result has already been shown to be appropriate for organic single crystals in Chapter 2. In the case of polymer crystals, two of the surfaces will contain chain folds having significantly different energies from the others; for polyethylene the specific surface energy (σ_e) of the folded surfaces is about 60–70 mJ m^{-2} which is about five times greater than the value for the surface containing the aligned chains (σ) which has a value of about 15 mJ m^{-2}. The ratio of the equilibrium thickness (along the chain axis direction) to the width perpendicular to the chain direction is consequently close to > 5. The predicted value of this ratio being > 5 is three to four orders of magnitude greater than that observed experimentally.[6] The difference between experiment and prediction could be a consequence of crystals not being in equilibrium with the melt and that crystals will rearrange when given enough 'thermal stimulation'. In Chapter 4 we noted that just below the melt temperature hydrocarbon chains have a relatively high degree of rotational mobility and this is associated with the plastic crystalline phase in these materials. It is therefore not unreasonable to expect that similar mobility would aid rearrangement of the crystal chains in the newly formed surface. In Chapter 5 it was noted that on thermal annealing, thickening of lamellae occurs. The thickness of solution-grown lamellae (L_c^*) depends on the degree of supercooling ($\Delta T = T_m^0 - T_c$, where T_m^0 is the equilibrium melting point and T_c is the

crystallization temperature):[6]

$$L_c = \frac{C_1}{\Delta T} + \delta L \tag{6.7}$$

where C_1 and δL are constants for a particular polymer system. The effect of supercooling on the lamella thickness for the case of linear polyethylene[7–10] and similar regular polymers is shown in Figure 6.2.

The Thompson–Gibbs (TG) equation (4–6) allows the melting point to be related to the lamella thickness. The change in free energy on melting (ΔG_m) is given by

$$\Delta G_m = \Delta G^* + \sum_{i=1}^{n} A_i \sigma_i \tag{6.8}$$

where ΔG^* is the surface-independent change in free energy and σ_i is the specific surface energy of surface i with area A_i. At equilibrium:

$$\Delta G_m = 0 \Rightarrow \Delta G^* = \sum_{i=1}^{n} A_i \sigma_i \tag{6.9}$$

For a simple polymer crystal, the lamellae dominate the growth and the two surfaces that contain the folded chains dominate the total surface energy term. It can be assumed that there is a free energy term that is independent of this fold surface and represents the interaction between the all-*trans* linear chains, *stems*, and has the form

$$\Delta G^* = \Delta G_B^* A L_c \rho_c \tag{6.10}$$

where ρ_c is the density of the crystal plane. Both ΔH_B and ΔS_B can be regarded as temperature-independent bulk parameters, and the specific bulk free energy

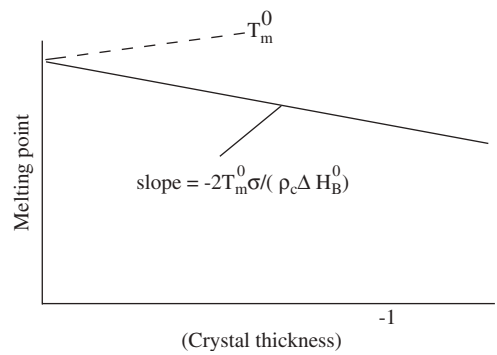

Figure 6.2 Schematic plot of the variation of the melting point with the reciprocal of the crystal thickness.

change (ΔG_B^*) is given by

$$\Delta G_B^* = \Delta H_B^0 - T_m \Delta S_B^0 = \Delta H_B \left(1 - \frac{T_m}{T_m^0}\right) = \Delta H_B \left(\frac{T_m^0 - T_m}{T_m^0}\right) \tag{6.11}$$

By inserting eqn (6.11) into eqn (6.10), the following equation is obtained:

$$\Delta G^* = \Delta H_B^0 (T_m^0 - T_m) \frac{A L_c \rho_c}{T_m^0} \tag{6.12}$$

Inspection of the lamellae would indicate that the surfaces containing the chain *stems* are usually the short sides and have a small area compared with the sides that contain the folded chains. As indicated previously, it is the surfaces that contain the folded chains that make the major contribution to the surface free energy. It is therefore appropriate to assume that the total area of the four lateral surfaces is small compared to the area of the fold surfaces and the contribution to the total surface free energy of the crystal can be neglected:

$$\sum_{i=1}^{n} A_i \sigma_i \approx 2\sigma A \tag{6.13}$$

Combination of eqn (6.9), (6.12) and (6.13) gives

$$\Delta H_B^0 (T_m^0 - T_m) \frac{A L_c \rho_c}{T_m^0} = 2\sigma A$$

$$T_m^0 - T_m = \frac{2\sigma A T_m^0}{A L_c \rho_c \Delta H_B^0} = \frac{2\sigma T_m^0}{L_c \rho_c \Delta H_B^0} \tag{6.14}$$

which may be simplified to give the Thompson–Gibbs equation:

$$T_m = T_m^0 \left(1 - \frac{2\sigma}{L_c \rho_c \Delta H_B^0}\right) = \frac{-2 T_m^0 \sigma}{\rho_c \Delta H_B^0} \tag{6.15}$$

The Thompson–Gibbs equation predicts a linear relationship between the melting point and the reciprocal of the crystal thickness (Figure 6.2). In practice, it is difficult to obtain the melting point and crystal thickness data, as the experiments involved in determining the melting point allow crystal thickening to occur.

6.3 Nature of Chain Folding

If chain folding were regular and the chain *stems* were to lie adjacent to one another then the density would be close to that predicted from the crystal lattice

structure. In Chapter 5, it was identified that small distortions of the lattice can be observed. Further, measurement of any crystalline polymer will indicate that the density is less that that from the predictions for the perfect crystalline material, indicating the presence of amorphous material. It is proposed that part of the amorphous content arises from disorder: irregular folding of the polymer chains (Figure 6.3).

The irregular folds in which the chains do not re-enter the lamellae at the next layer lead to the concept of the so-called switchboard model.[11] Early telephone switchboards were formed from a matrix of connections into which a connecting cable could be plugged. It was therefore possible to connect adjacent points—tight re-entry—or in a random fashion. Flory[11] argued that *random* re-entry was normal and regular, tight folding was rare. His argument was based on the melt behaviour where the polymer chains follow closely random coil statistics and the RISM model[1] has been every successful. It is only with the advent of small-angle neutron scattering (SANS) of blends of deuterated and protonated polymers, e.g. $(–CD_2–)_n$ and $(–CH_2–)_n$, that the validity of this model can be tested.[12]

For solution-grown single crystals of linear polyethylene,[13] the average radius of gyration ($<s>$) of the molecules is proportional to $M^{0.1}$. A much greater molar mass dependence of $<s>$ is observed for the polymer coil in solution, $<s> \propto M^{0.5}$, and indicates that the dimensions of the chains decrease markedly during crystallization. For the polymer chains to have a smaller value of $<s>$ they have to fold like an accordion and the *gauche* sequences have to be closely coupled in order to achieve close packing.

Flory based his ideas of re-entry on the tried and tested assumption that the coil follows random coil statistics in the melt. It is clear from the SANS data that the chains fold much more tightly than would be predicted by a random re-entry model.[14] Infrared spectroscopy showed that 75% of the folds

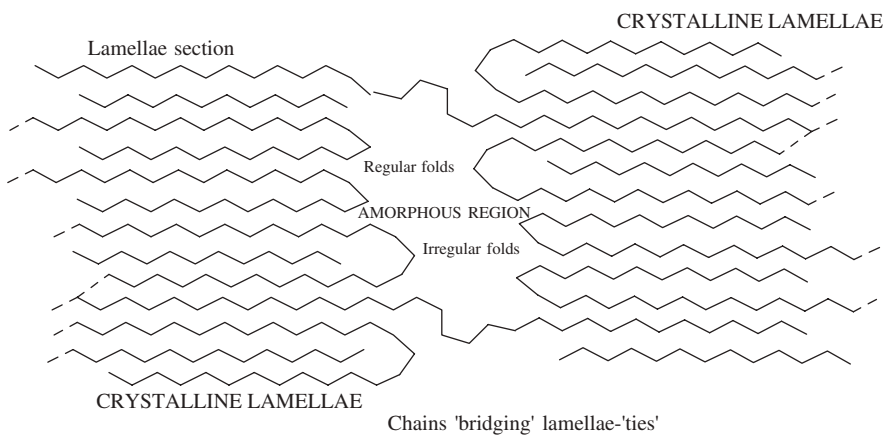

Figure 6.3 Schematic of a folded surface showing regular folds, irregular folds and bridging 'tie' molecules.

in solution-grown single crystals of polyethylene led to adjacent re-entry (tight folds) and that single molecules were diluted by 50% along the 110 fold plane. Both observations are consistent with the *super-fold* model where the chains behave more like the regular folds than the random re-entry model.

6.4 Crystals Grown from the Melt and Lamellae Stacks

The *super-folding* model indicates that in dilute solution the polymer molecules add to the growing face of a single crystal without significant competition from other polymer molecules. Crystal growth in concentrated solutions and the melt will be very different and chain entanglement will influence the growth process. When polymers are entangled, then the possibility arises of several chains adding to the surface at the same time and the process becomes more chaotic and the folding behaviour may tend more towards the switchboard model.[11] In general, low molecular weight polyethylene, because it is not entangled, can readily crystallize, exhibiting a well-defined lamellar morphology with a thickness-to-width ratio of 0.001–0.01. The lamellae often align parallel to one another forming regular stacks. This behaviour is particularly apparent with metallocene polyethylene, where there are very few branched chains to inhibit chain folding. The lamellae formed with low molecular weight materials can exhibit thickness-to-width ratios which are smaller than 0.001. Once entanglement can occur then growth of the large lamellae is inhibited and smaller less regular lamellae are usually observed. Branched and/or high molar mass polymers exhibit lamellae that tend not to be able to form regular stacks and exhibit much higher ratios. As discussed in Chapter 5, the lamella distortions can lead to characteristic shaped crystals. The regular tight-folded lamellae can form roof-shaped lamellae, pyramidal structures, whereas intermediate molar mass materials tend to form C-shaped lamellae and high molar mass polymers form S-shaped lamellae. Branching will introduce defects and, depending on its location and the length of the branches, different effects on the lamellae growth process will occur. The incorporation of the branches will impart curvature to the lamellar crystal sheets. Branched polyethylene shows mostly C- and S-shaped lamellae.

Polymers are always polydisperse with a distribution in molar mass and often contain chain branches, either introduced specifically during synthesis or as a consequence of synthetic defects, and both these effects will influence the observed morphology. As we shall see later, copolymers are a special case; however, the introduction of low levels of comonomers can lead to behaviour which is rather like that of random branched chains. Different molecular species crystallize in different stages indicating the thermodynamic control on the overall process, *i.e.* they are incorporated into the crystal structure at different temperatures and times. The intermediate and high molar mass component crystallizes early in the stacks of thick dominant crystals. Small pockets of rejected molten low molar mass material remain after crystallization

of the dominant lamellae. The low molar mass species crystallize in separate crystal lamellae, favouring stacks of so-called subsidiary crystal lamellae. The process leading to separation of high and low molar mass material that accompanies crystallization is referred to as a molar mass segregation or fractionation. Some polymers show a preference for segregation of low molar mass species to the spherulitic boundaries.

For melt-grown polymers the amorphous density is 10–20% lower that the crystal density. Flory argued that all the chains entering the amorphous phase would take a random walk before re-entering the crystal lamellae. A significant fraction of the chains must, however, be fold directly back into the crystal in order to account for the observed low amorphous density.

An expression can be derived for the fraction of tight folds. Usually it is assumed that all of the chains can be divided into two groups: those that form tight folds and those that do not. The latter are assumed to exhibit random re-entry behaviour. In Figure 6.3 the tight regular folds have a density that is essentially that of the lamellae and the irregular folds are much bigger, entering further into the amorphous region and exhibiting random re-entry behaviour. If the length of chain between the lamellae is designated L_a, and there are n bonds in a typical Gaussian amorphous chain sequence, then

$$n = \frac{L_a^2}{Cl^2} \tag{6.16}$$

where C is a characteristic constant for a given polymer–temperature combination and l is the monomer bond length. Regular chain folding constitutes a fraction (f_{fold}) of the entries and these will *not* contribute to the fraction of the amorphous chains. The number of chain segments in an average amorphous entry is given by

$$n = \frac{L_a^2}{Cl^2}(1 - f_{fold}) \tag{6.17}$$

The number of chain segments (n^0) in a straight chain, *stem*, is given by

$$n^0 = \frac{L_a}{l} \tag{6.18}$$

The ratio of segments in the two phases will be in the ratio of the amorphous (ρ_a) to crystalline density (ρ_c):

$$\frac{\rho_a}{\rho_c} = \frac{n}{n^0} \tag{6.19}$$

The amorphous density is then obtained by a combination of eqn (6.17)–(6.19):

$$\rho_a = \rho_c \frac{L_a}{Cl}(1 - f_{fold}) \tag{6.20}$$

Careful X-ray diffraction studies have shown that the chains do not match exactly and as a consequence they are tilted by an angle θ.[15–17] To allow for this effect, eqn (6.20) can be modified to give

$$\rho_a = \rho_c \frac{L_a}{Cl}(1 - f_{fold}) \cos\theta \tag{6.21}$$

For a typical linear polyethylene the ratio for the densities ρ_a/ρ_c is 0.85 and the amorphous distance is approximately 5 nm and l has a value of 0.127 nm. The value of C is 6.85 and $\theta = 30^\circ$; using these data the value of f_{fold} is 0.83; *i.e.* 83% of all chain stems are expected to be tightly folded and 17% are expected to be statistically distributed chains in the amorphous layer. The amorphous phase can have a dominating influence on the physical properties of many semi-crystalline polymers, determining the ultimate strength, ductility and diffusion coefficients for small molecules. The strength and ductility of semi-crystalline polymers of high molar mass arise from the presence of interlamellar tie chains connecting adjacent crystal lamellae and are critical in determining the resistance to environmental stress cracking.

6.4.1 Location of Chain Ends

Any discussion of the lamellar structure raises the following question: where are the chain ends?

In Figure 6.3 some of the chain ends are shown to be close to the surface of the crystal. Keller and Preist have shown that about 90% of the chain ends are located in the amorphous phase, surface, of the lamellae. The concentration of interlamellar *tie* chains in a given sample depends on molar mass that in turn determines the spatial distribution of the chains and long period, *i.e.* the sum of crystal and amorphous layer thickness. If the polymer chains are shorter than the critical length for entanglement, then the chains can act independently and become separately incorporated in the lamellae. For low molar mass chains where their length is twice as long as the long period, the chains will fold into the same lamellae and there will be few bridging *tie* molecules and a brittle crystalline material will develop. Once more we must recall that the chains in the newly formed surface can probably undergo significant rearrangement and the lower energy state of a chain end in the surface can be rapidly achieved. For high molecular mass materials, an increasing proportion of the chains will leave one lamella and enter the adjoining lamella. The bridging section will often be entangled and the *tie* molecules will add to the strength of the material.

6.5 Crystallization Kinetics[6]

A core assumption when discussing the crystallization kinetics of polymers is that the theories must consider the effects of chain folding. In Chapter 2 the principles of crystallization were outlined and the importance of the differences

in the energy of the surface to which the molecules were being attached was demonstrated. The same basic principles apply to polymer crystals except that now the entity that is being attached is a polymer chain. In principle, Monte Carlo simulations can predict the growth process in a manner similar to that used for small molecules; however, some of the more empirical theories help the experimentalist gain an appreciation of the mechanism of the processes involved in practice.

As in the case of small molecules, the crystallization process involves nucleation and diffusion of the relevant entity to the surface site. The formation of the critical nucleus will be controlled by thermodynamics. The total change in free energy ΔG is the sum of contributions from the bulk and surface energies. Using the convention which we introduced in Figure 6.1, where σ_i is the specific surface energy of surface i and A_i is the area, then the free energy can be described by

$$\Delta G = \Delta G_{\mathrm{B}} V_{\mathrm{crystal}} + \sum_i A_i \sigma_i \tag{6.22}$$

where ΔG_{B} is the change in the specific free energy in transformation of stems from the solid to the melt and V_{crystal} is the volume of the crystal. For simplicity it will be assumed that the crystal being considered has a spherical form. The free energy on crystallization (ΔG) is then given by

$$\Delta G = \frac{4\pi r^3}{3} \Delta G_{\mathrm{B}} + 4\pi^2 \sigma \tag{6.23}$$

where r is the radius of the spherical crystal and σ is the average specific free energy of the surface. The radius of the sphere (r^*) associated with the free energy barrier is obtained by setting the derivative of ΔG with respect to r equal to zero:

$$\frac{\partial \Delta G}{\partial r} = 4\pi^{*2} \Delta G_{\mathrm{B}} + 8\pi r^* \sigma = 0 \tag{6.24}$$

where

$$r^* = \frac{2\sigma}{\Delta G_{\mathrm{B}}} \tag{6.25}$$

The temperature dependence of this equation lies in ΔG_{B}:

$$\Delta G_{\mathrm{B}} = \frac{\Delta H_{\mathrm{B}}^0 \Delta T}{T_{\mathrm{m}}^0} \tag{6.26}$$

where ΔH_{B}^0 is the heat of fusion per unit volume, I_{m}^0 is the equilibrium melting point, $\Delta T = T_{\mathrm{m}}^0 - T_{\mathrm{c}}$ is the degree of *supercooling* and T_{c} is the crystallization temperature. Equation (6.26) is valid provided that ΔH_{B}^0 and the entropy of fusion, ΔS_{B}^0, are temperature independent, which is a good approximation over a limited temperature range near the equilibrium melting temperature.

Insertion of eqn (6.26) into eqn (6.25) yields

$$r^* = -\frac{2\sigma T_m^0}{\Delta H_B^0 \Delta T} \tag{6.27}$$

Since ΔH_B^0 is negative, the radius of the critical nucleus increases with decreasing degree of *supercooling*. Inserting eqn (6.27) into eqn (6.23) gives an expression for the free energy barrier (ΔG^*):

$$\Delta G^* = \frac{4\pi\left(-2\sigma T_m^0\right)^3}{3\left(\Delta H_B^0 \Delta T\right)^3}\frac{\Delta H_B^0 \Delta T}{T_m^0} + \frac{4\pi\left(-2\sigma T_m^0\right)^2\sigma}{\left(\Delta H_B^0 \Delta T\right)^2} \tag{6.28}$$

which simplifies to

$$\Delta G^* = \frac{16\pi\sigma^3 (T_m^0)^2}{3(\Delta H_B^0)^2 \Delta T^2} \tag{6.29}$$

Equation (6.29) predicts that nucleation occurs more readily at lower crystallization temperatures because of the lower critical nucleus size and the lower free energy barrier associated with the crystallization process. As with the case of simple crystal growth, nucleation can take a number of forms:

- Primary nucleation that involves the formation of the first nuclei and involves six new surfaces being formed.
- Secondary nucleation will usually occur on a surface and typically involves four surfaces being formed.
- Tertiary nucleation involves typically two surfaces being formed and represents the stem attaching to an edge face.

The various forms of nucleation are schematically presented in Figure 6.4. By analogy with case of small crystals (Chapter 2), the free energy barrier is highest for primary nucleation and this seldom occurs in practice, heterogeneous nucleation being the normal mechanism.

It has been proposed that the following equation can be used to describe the temperature dependence of both diffusive transport and nucleation. The overall crystallization rate ($\dot{w}_c$) at a general temperature (T_c) is a combination of several factors. The crystallization process involves the diffusion (the first

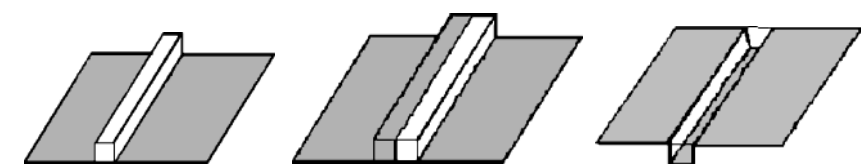

Figure 6.4 Schematic of the types of nucleation for stems adding to a crystal surface. The *stem* adding to the surface is shown in white except in the tertiary case where the addition is to the trough.

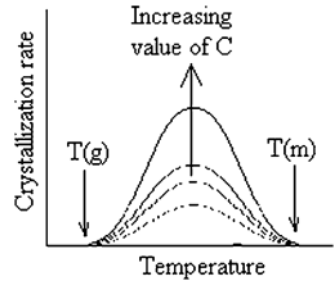

Figure 6.5 Variation of the crystallization rate with temperature. T_g and T_m are, respectively, the glass and melt temperatures of the material.

exponential term) of the stem to the surface and then its nucleation (the second exponential term) or attachment:

$$(\dot{w_c}) = C \exp\left(-\frac{U^*}{R(T_c - T_\infty)}\right) \exp\left(-\frac{K_g}{T_c(T_m^0 - T_c)}\right) \tag{6.30}$$

where C is a rate constant, U^* is an energy constant, R is the gas constant, T_∞ is the temperature at which all segmental mobility is frozen in and K_g is a kinetic constant for the secondary nucleation.

The pre-exponential factor C depends on the regularity and flexibility of the polymer segments and will be a large value for a flexible all-*trans* polymer, $C = 0$ for an atatic polymer and is low for an inflexible polymer such as isotactic polystyrene. The second term in eqn (6.30) describes the temperature dependence of the short-range motion of the stems to the surface and is expressed by the Williams–Landau–Ferry (WLF) equation.[17] The WLF equation describes the slowing down of the segmental motion of the chain backbone at the glass transition temperature and reflects the restriction on the volume available for motion to occur. At $T_c = T_\infty$ this term becomes zero. The third term describes the temperature dependence of the nucleation rate and has a zero value above the equilibrium melting temperature $T_c = T_m^0$. The form of the temperature dependence of the rate of crystallization is shown in Figure 6.5. It is a bell-shaped curve.

The form of the crystallization rate curve is common to many systems and similar expressions have been found for metals, inorganic compounds, sulfur, selenium, antimony, proteins and carbohydrates, graphite silicates and also polymers.

6.6 Equilibrium Melting Temperature

Central to most crystallization is the idea of an equilibrium melting temperature, T_m^0, above which crystallization does not occur. The rate of crystal growth is therefore related to the extent to which supercooling (ΔT) occurs and is defined by

$$\Delta T = T_m^0 - T_c \tag{6.31}$$

where T_c is the crystallization temperature. The equilibrium melting temperature for a polymer system normally refers to the growth of a theoretical crystal of infinite thickness in which the chains are fully extended. Homopolymers of intermediate or high molar mass can grow crystals of practically infinite thickness. The fully extended chain length of a polyethylene of $M = 100\,000$ g mol^{-1} is $100\,000/14 \times 0.127$ nm $\sim$ 900 nm and is several orders of magnitude larger than the thickness of the lamellae.[6] The usual dimensions are $\sim$10 nm, and for these dimensions to be achieved chain folding must occur. The melting point depression arising from the finite crystal thickness (900 nm) predicted by the Thompson–Gibbs equation (eqn (6.15)) is in this case negligible. However, low molar mass homopolymers can obviously grow crystals of only a limited thickness equal to their fully extended length (Chapter 2). The melting point of these materials does correspond to the predictions for the fully extended chain. Copolymers are more complicated, the change in the chemical sequence structure representing a disruptive element inhibiting chain packing. Depending on the nature of the comonomer, the 'foreign' moieties with a 'statistical' placement in the polymer chains may be fully non-crystallizable or they may be included to some extent in the crystals. As a consequence the equilibrium thickness will reflect the disruptive effects of these moieties. Very large lamellae are found in highly linear polymers such as certain metallocene-synthesized polyethylenes.

An example of the effect of different crystallization temperatures on the melt temperature for poly(trimethylene terephthalate) is shown in Figure 6.6. The value of T_m^0 is equal to 245.6 °C. The data follow a good linear variation of the melting temperature with the crystallization temperature.

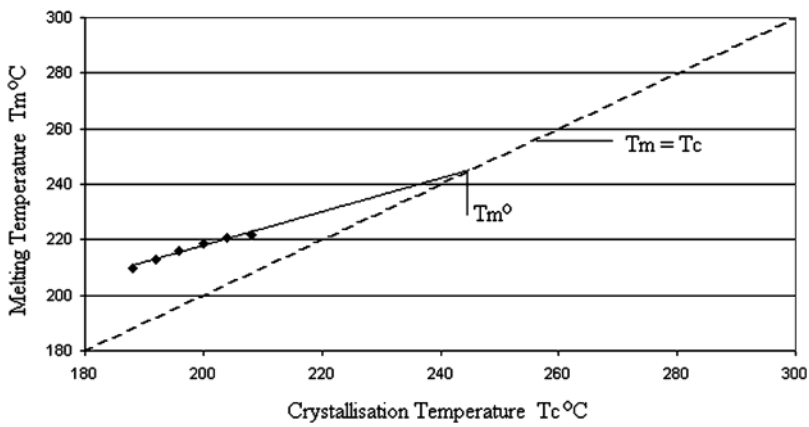

Figure 6.6 Variation of melting temperature with crystallization temperature for poly(trimethyl terephthalate) (unpublished data, A. Mckintosh and J. J. Liggat).

The equilibrium melting temperature can be determined in a number of different ways. The melting point (T_m) of samples with a well-defined crystal thickness (L_c) can be measured and the data extrapolated to $L_c^{-1} = 0$ using the Thompson–Gibbs equation:

$$T_m = T_m^0 \left[1 - \frac{2\sigma}{\Delta H_B^0 \rho_c L_c}\right] \tag{6.32}$$

where ρ_c is the crystal density, ΔH_B^0 is the heat of fusion per unit mass and σ is the specific fold surface energy. Certain polymers, such as polyethylene, can be crystallized at elevated pressures to form extended chain crystals and these micrometre thick crystals have melting points that are close to the theoretical value of T_m^0.

An alternative approach is to derive the value of T_m^0 from a study of low molar mass analogues and then extrapolate to the infinitely thick crystal value. Using data for the enthalpy (ΔH_B) and entropy (ΔS_B) of fusion for oligomers, T_m^0 is obtained by extrapolation to infinite molar mass and for linear polyethylene has the form

$$T_m = 414.3\left[\frac{x - 1.5}{x + 5.0}\right] \tag{6.33}$$

where x is the degree of polymerization of the polymer. For high molecular mass materials this melting point has a limiting value of 414.3 K. Similar relationships have been observed for other polymer systems. Equilibrium melting points of a few selected polymers are presented in Table 6.1.[4–6]

It is clear from these examples that there is no correlation between the melting temperature and the enthalpy of fusion. The values of ΔH_B clearly do

Table 6.1 Equilibrium melting point and selected thermodynamic data for various polymers.[6,18]

Polymer	T_m^0 *(K)*	ΔS_B^0 *(J K^{-1} mol^{-1})*	ΔH_B^0 *(kJ mol^{-1})*
Polyethylene	414	9.6	4.01
Polytetrafluoroethylene	600	5.7	3.42
Isotactic polypropylene	463	7.5	2.31
Polyoxymethylene	457	10.7	4.98
Poly(ethylene oxide)	342	8.4	2.89
Nylon 6,6	553	10.2	4.85
Poly(1,4-*cis*-isoprene)	301	14.5	4.39
Poly(1,4-*trans*-isoprene)	347	36.6	12.70
Poly(1,4-*trans*-chloroprene)	353	23.7	8.36
Isotactic polystyrene	516	16.3	8.38
Poly(decamethylene adipate)	352.5	121.2	42.64
Poly(decamethylene sebacate)	353	142.1	50.16
Poly(tetramethylene terephthalate)	411	63.1	31.76
Cellulose tributyrate	480	33.8	12.54

not dictate the values of the melt temperature and it is rather the balance between the enthalpy and entropy that is the controlling factor.

Nylon 6,6 has a high enthalpy of fusion due to the strong hydrogen bonds between amide groups. In contrast, the higher melting point of polytetrafluoroethylene (PTFE) is due to its low entropy of fusion. At high temperature, PTFE crystals show considerable segmental mobility that leads to a relatively small increase in entropy on melting.

PTFE also exhibits a lattice change in the solid state just below its melting point, rather like the plastic phase transition discussed in Chapter 4. This lattice change is consistent with a high mobility in PFTE below its melting point. The high melting point of polyoxymethylene (POM) is due to the high enthalpy of fusion arising from intermolecular interactions involving the ether groups. The addition of the extra methylene group in poly(ethylene oxide) (PEO) leads to a reduction of the effects of the ether groups and a consequent reduction in the enthalpy of fusion. The introduction of a ring structure into a linear chain substantially increases the melting temperature relative to the aliphatic chain as would be expected from the decreased conformational entropy of the melt. Striking examples of this phenomenon are found in comparisons of the melting temperature of aliphatic and aromatic polyesters and polyamides. Cellulose derivatives usually have a highly extended structure with low entropy and consequently have high melting points. From the few examples presented it is apparent that the chain structure influences the melting temperature through its conformational properties.

6.7 General Avrami Equation

A generalized approach to the description of the crystallization process was proposed by Avrami.[19–21] Without prior knowledge of the molecular mechanism involved in the crystallization process, the Avrami equation gives a convenient means of empirically describing crystallization. The model assumes that crystallization starts randomly throughout the sample, which since nucleation is often heterogeneous, is a good approximation to reality. The theory attempts to accommodate the effects of the growth rate on the shapes of the crystals that are formed. It is assumed that the crystals that are seeded will grow smoothly in all three dimensions. All nuclei are formed and start to grow at time $t = 0$ and with a rate that is the same in all directions (spherical growth) and is equal to $\dot{\omega}$. The theory considers the growth front, $E(t)$, emanating from the central nucleus which will be described:

$$E(t) = \frac{4}{3}\pi(\dot{\omega}t)^3 q \tag{6.34}$$

where q is the volume concentration of nuclei. Statistical analysis of the crystal growth problem can be considered in terms of an expanding circular wave front that mimics spherulite growth. The number of waves that pass a particular point

at time t can be described in terms of a Poisson distribution that has the form

$$p(c) = \frac{\exp(-E)E^c}{c!} \tag{6.35}$$

where E is the average value of the number of waves passing a point P after some time t and the number of waves are constrained to be an exact number c. The probability that no fronts pass the point P is given by

$$p(0) = \exp(-E) \tag{6.36}$$

In the context of the crystallization process, $p(0)$ is equivalent to the volume fraction $(1 - v_c)$ of the polymer which is still in the molten state:

$$p(0) = 1 - v_c \tag{6.37}$$

where v_c is the volume fraction of crystalline material. Combination of eqn (6.34) with eqn (6.37) yields

$$1 - v_c = \exp\left(-\frac{4}{3}\pi\dot{\omega}^3 q t^3\right) \tag{6.38}$$

This equation indicates that in the case of spherical growth the growth rate depends on the cube of the time.

If now the growth rate is assumed to be constant and linear in space and time then the number of waves (dE) which pass the arbitrary point (P) for nuclei within the spherical shell confined between the radii r and $r + dr$ is given by

$$dE = 4\pi r^2\left(t - \frac{r}{\dot{\omega}}\right)I^* dr \tag{6.39}$$

where I^* is the density, the number of nuclei per cubic metre per second. The total number of passing waves (E) is obtained by integration of dE between 0 and $\dot{\omega}t$:

$$E = \int_0^{\dot{r}t} 4\pi r^2 I^*\left(t - \frac{r}{\dot{\omega}}\right) dr = \frac{\pi I^*\dot{\omega}^3}{3} t^4 \tag{6.40}$$

which, after insertion into eqn (6.36) and (6.37) gives

$$1 - v_c = \exp\left(-\frac{\pi I^*\dot{\omega}^3}{3} t^4\right) \tag{6.41}$$

It should be noted that now the time is raised to the fourth power. In general it is found that crystallization based on different nucleation and growth mechanisms can be described by the same general formula, the general Avrami equation:

$$1 - v_c = \exp(-Kt^n) \tag{6.42}$$

where K and n are constants typical of the nucleation and growth mechanisms. The growth geometry describes the characteristics of the dominant process.

Equation (6.42) can be expanded according to $\exp(-Kt^n) \approx 1 - Kt^n + \ldots$ and for the early stages of crystallization where there is little restriction of crystallization due to impingement:

$$v_c = Kt^n \tag{6.43}$$

The Avrami exponent (n) increases with increasing 'dimensionality' of the crystal growth (Table 6.2). Diffusion-controlled growth reduces the value of the exponent by a factor of 1/2 compared with the corresponding 'free' growth case. There are certain limitations and special considerations for polymers with regard to the Avrami analysis:

(i) The solidified polymer is always only semi-crystalline because, as discussed previously, the crystals are never 100% perfect or completely volume filling. This effect can be taken into account by a modification of eqn (6.43) to

$$1 - \frac{v_c}{v_{c\infty}} = \exp(-Kt^n) \tag{6.44}$$

where $v_{c\infty}$ is the volume crystallinity finally reached.

(ii) The volume of the system studied changes during crystallization as a consequence of the difference in density between the melt and the solid:

$$1 - v_c = \exp\left\{-K\left[1 - v_c\left(\frac{\rho_c - \rho_l}{\rho_l}\right)\right]t^n\right\} \tag{6.45}$$

where ρ_c is the density of the crystal phase and ρ_l is the density of the melt.

(iii) The nucleation is seldom either athermal or simple thermal. A mixture of the two is common.

(iv) Crystallization always follows two stages: (1) primary crystallization, characterized by radial growth of spherulites or axialites; and (2)

Table 6.2 Avrami exponent n for different nucleation and growth mechanisms.[4]

Growth geometry	*Athermal*	*Thermal*[a]	*Thermal*[b]
Linear growth	1	2	1
Two-dimensional, circular	2	3	2
Three-dimensional			
Spherical	3	4	5/2
Fibrillar	≤ 1	≤ 2	
Circular lamellar	≤ 2	≤ 3	
Solid sheaf	≥ 5	≥ 6	

[a] Free growth: $\dot{\omega} =$ constant.
[b] Diffusion-limited growth: $\dot{\omega} \propto 1/\sqrt{t}$.

secondary crystallization, *i.e.* the slow crystallization behind the crystal front caused by crystal thickening, and the formation of subsidiary crystal lamellae from secondary crystallization is associated with the fractionated low molar mass material and results in crystal imperfections.

The constants in the Avrami equation are obtained by taking the double logarithm of eqn (6.44):

$$\ln\left[-\ln\left(1-\frac{v_c}{v_{c\infty}}\right)\right] = \ln K + n\ln t \tag{6.46}$$

Differential scanning calorimetry (DSC) can be used to study the crystal growth kinetics. The nature of the experiment leads to data that are defined in terms of mass rather than volume. In order to convert the data the following expression is used to relate the mass crystallinity (w_c) to a volume fraction (v_c):

$$v_c = \frac{w_c/\rho_c}{\frac{w_c}{\rho_c}+\frac{(1-w_c)}{\rho_a}} = \frac{w_c}{w_c+\frac{\rho_c}{\rho_a}(1-w_c)} \tag{6.47}$$

where ρ_a is the amorphous density. Typically the theory is found to fit well the initial crystallization data but deviations are observed once the growth effects of neighbouring entities start to impinge.

6.8 Comparison of Experiment with Theory

Studies of low molar mass polyethylene, $\bar{M}_c \leq 10\,000$, show an exponent of 4 consistent with the theory for spherulitic growth.[22,23] The low molar mass samples display sheaf-like (axialitic) morphology and as expected a high value of the exponent is observed. Polymers with intermediate molar mass, $10\,000 < \bar{M}_w < 1\,200\,000$, have an Avrami exponent near 3 and for higher molar mass samples, $\bar{M}_w \geq 3\,000\,000$, the exponent is further reduced to a value of ~ 2. These observations are consistent with growth occurring predominately in one direction. The crystallization of high molar mass polymers is strongly influenced by chain entanglements and the slow and incomplete crystallization leads to small, uncorrelated crystals, *i.e.* to so-called random lamellar structures. A low value of n is expected for such a 'low-dimensional' platelet or fibrillar-like growth. It is common to observe that the Avrami exponent decreases with increasing molar mass reflecting the influence of the differences in morphology and crystal growth mechanisms on the observed behaviour.

6.9 Growth Theories

As in the case of small molecules, attempts have been made to develop theories that help to probe the mechanism of crystal growth. As with small molecules

(Chapter 2), theories can be divided into equilibrium and kinetic theories. Kinetic theories are principally of two types: enthalpic nucleation theories and entropic theories. Nucleation theories, e.g. the Lauritzen–Hoffman (LH) theory,[5,24,25] assume that the free energy barrier associated with nucleation has an energetic origin. The Sadler–Gilmer theory[12,26] regards the free energy barrier as predominantly entropic. Kinetic theories predict the temperature dependence of growth rate, initial crystal thickness (L_c^*) and other morphological parameters.

6.9.1 Lauritzen–Hoffman Theory[5,25]

The theory assumes that the spherulites or axialites grow radially at a rate-which is a function of the degree of supercooling, $\Delta T = T_m^0 = T_c$, where T_m^0 is the equilibrium melting point and T_c is the crystallization temperature. The basic assumptions are similar to those of the Avrami theory: growth occurring at a linear rate. Secondary or tertiary nucleation is assumed and involves only relatively short-range diffusion of the crystallizing units (*stems*). The theory assumes that a secondary nucleus is firstly formed (Figure 6.7) and subsequent *stems* are attached to the surface at a rate ω_s. The thickness of the extended element of the polymer chain, *stem*, along the growth direction is b. As in the case of small molecules, the attachment may be initially to the crystal surface and it then diffuses to an edge, where stable growth will occur.

The rate at which the first *stem* is attached, A_0, will be different from the rest as indicated in Figure 6.5 and leads to a difference in the free energy change (Figure 6.8). The associated free energy change (a) is the sum of a contribution due to covering the crystal surface plus part of the free energy of crystallization. The first *stem* only effectively has interaction through one surface. The attachment of the second *stem* will involve the formation of the first fold and the interaction between the *stem* is between the crystal surface and the first *stem* which leads to a reduction in the free energy for formation. Each additional

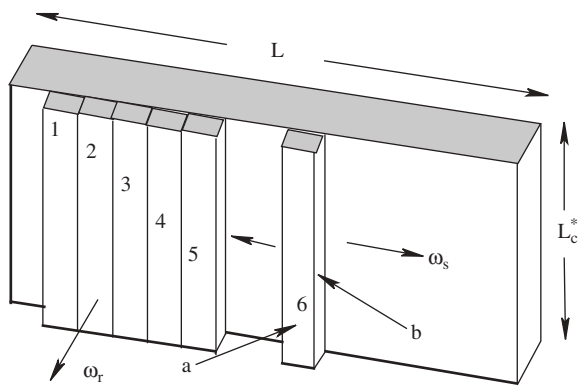

Figure 6.7 Growth processes on a crystal surface. Stem (6) is attached and will diffuse to the growing surface represented by stems (1)–(5). Stem (1) is assumed to be the first attached to the surface.

attachment will involve the creation of a further fold as indicate by the difference between (b) and (c).

The change in free energy involves the surface free energy ($2bL_c\sigma_L$) reduced by a fraction of the free energy of crystallization ($\psi 2bL_c\sigma_L$). The process is schematically described in Figure 6.8. The value of the free energy ΔG for the process is defined as being positive for $T_c < T_m^0$. The remainder of the free energy of crystallization ($(1 - \psi)2bL_c\sigma_L$) for the first *stem* is released on the other side of the maximum. The next process involves the formation of the first fold ($2ab\sigma$) that is accompanied by the release of a fraction of the free energy of crystallization ($\psi abL_c\Delta G$). On the rear side of the second maximum, the rest of the free energy of crystallization of the second *stem* is released. Later crystallizing *stems* exhibit the same energy barriers as the second stem (Figure 6.8).

The rate of deposition of the first stem is

$$A_0 = \beta \exp\left[-\frac{2bL_c\sigma_L - \psi abL_c\Delta G}{kT_c}\right] \tag{6.48}$$

where

$$\beta = \left(\frac{kT_c}{h}\right) J_1 \exp\left[-\frac{U^*}{R(T_c - T_\infty)}\right] \tag{6.49}$$

As indicated above, the term β allows for the diffusion of the *stem* to the site and is usually described by the WLF equation, h is Planck's constant, J_1 is a dimensionless scaling constant, U^* is a constant (dimensions J mol^{-1}) and T_∞ is the temperature at which diffusion is stopped. If the polymer is of sufficiently high molar mass for entanglement to take place, then instead of the WLF theory the reptation theory of de Gennes[27] should be used:

$$\beta = \left(\frac{kT_c}{h}\right)\left(\frac{1}{\overline{M_z}}\right) \exp\left(-\frac{\Delta E_r}{RT_c}\right) \tag{6.50}$$

where ΔE_r is the activation energy for transport of a molecule undergoing reptation.

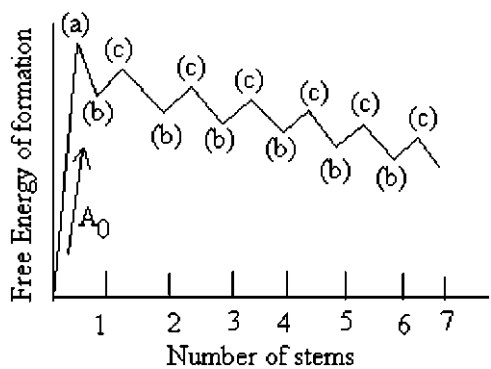

Figure 6.8 The free energy change associated with stem attachment.

The rate equations of the subsequent steps are

$$A = \beta \exp\left[-\frac{(2ab\sigma - \psi abL_c\Delta G)}{kT_c}\right] \tag{6.51}$$

$$B = \beta \exp\left[-\frac{[(1-\psi)abL_c\Delta G]}{kT_c}\right] \tag{6.52}$$

The ratios of A_0/B and A/B are independent of ψ. The absolute rate constants are dependent on ψ and the crystallization process involves subsequent addition of *stems* 1, 2, . . . , n to the substrate surface. If it is assumed that a steady-state condition is developed then:

$$\begin{aligned} S &= N_0A_0 - N_1B = N_1A - N_2B = \ldots \\ &= N_vA - N_{v+1}B \end{aligned} \tag{6.53}$$

Rearranging eqn (6.53) yields

$$N_{v+1} = \left(\frac{A}{B}\right)N_v - \frac{S}{B} \tag{6.54}$$

$$N_{v+1} = \left(\frac{A}{B}\right)^2 N_{v-1} - \frac{S}{B}\left(1 + \frac{A}{B}\right) \tag{6.55}$$

Further substitution of N_{v-1} finally leads to

$$S = N_0A_0\left(1 - \frac{B}{A}\right) \tag{6.56}$$

The equations describe the process of sequential addition of *stems* to the substrate. The initial *stems* are deposited and described by N_0A_0 and a balance will be achieved between the fraction of the *stems* that are permanently attached to the crystal and those that return to the melt by the ratio of the backward to the forward process, *i.e.* B/A.

By combining eqn (6.48)–(6.52) with eqn (6.56), the following expression is obtained:

$$\begin{aligned} S(L_c) = N_0\beta &\left[\exp\left(-\frac{(2bl_c\sigma_L - \psi abL_c\Delta G)}{kT_c}\right)\right] \\ &\times \left[1 - \exp\left(-\frac{(2ab\sigma - abL_c\Delta G)}{kT_c}\right)\right] \end{aligned} \tag{6.57}$$

This equation relates the rate of crystallization to its dependence on crystal thickness (L_c) and temperature (T_c). The average crystal thickness L_c^* can be

derived from the expression

$$L_c^* = \frac{\int_{L_c=2\sigma/\Delta g}^{\infty} L_c S(L_c)\,\mathrm{d}L_c}{\int_{L_c=2\sigma/\Delta g} S(L_c)\,\mathrm{d}L_c} \tag{6.58}$$

The lower limit of the above equation corresponds to the case of a crystal formed at the melting point:

$$L_{c,\min} = \frac{2\sigma}{\Delta G} = \frac{2\sigma T_m^0}{\Delta H^0 \rho_c (T_m^0 - T_c)} \tag{6.59}$$

and eqn (6.59) can be rearranged to give

$$T_c = T_m^0 \left[1 - \frac{2\sigma}{\Delta H^0 \rho_c L_{c,\min}}\right] \tag{6.60}$$

It is interesting to note that eqn (6.60) has an identical form to that of the Thompson–Gibbs equation. Note that ΔH^0 is the mass-related heat of fusion (in kg^{-1}) and that $T_c = T_m$. Integration of eqn (6.58) gives the expression

$$L_c^* = \frac{2\sigma}{\Delta G} + \frac{kT}{2b\sigma_L} \frac{\left[2 + \left(1 - 2\psi a \frac{\Delta G}{2\sigma}\right)\right]}{\left(1 - \frac{a\Delta G\psi}{2\sigma_L}\right)\left(1 + \frac{a\Delta G(1-\psi)}{2\sigma_L}\right)} \tag{6.61}$$

For $\psi = 1$ this reduces to

$$L_c^* = \frac{2\sigma}{\Delta G} + \frac{kT}{2b\sigma_L}\left[\frac{\left(\frac{4\sigma_L}{a} - \Delta G\right)}{\frac{2\sigma_L}{a} - \Delta G}\right] = \frac{2\sigma}{\Delta G} + \delta L_c \tag{6.62}$$

The parameter δL_c becomes infinite when

$$\Delta G = \frac{2\sigma_L}{a} \tag{6.63}$$

The degree of super cooling (ΔT_s) corresponding to the singularity can be derived as follows:

$$\frac{\Delta H^0 \rho_c \Delta T_s}{T_m^0} = \frac{2\sigma_L}{a} \Rightarrow \Delta T_s = \frac{2\sigma_L T_m^0}{a \Delta H^0 \rho_c} \tag{6.64}$$

For linear polyethylene and putting $\psi = 1$ yields the value of ΔT as 55 K. The singularity (or δL; catastrophe as it is sometimes called) may be avoided by

setting $\psi = 0$:

$$L_c^* = \frac{2\sigma}{\Delta G} + \frac{kT}{2b\sigma_L}\left[\frac{\left(\frac{4\sigma_L}{a} + \Delta G\right)}{\frac{2\sigma_L}{a} + \Delta G}\right] = \frac{2\sigma}{\Delta G} + \delta L_c \tag{6.65}$$

It must be remembered that the LH theory does not include any elements of crystal thickening and hence relaxation phenomena are not included. The LH theory introduces three possible growth regimes: I, II and III.

Regime I growth. It is assumed that in regime I (Figure 6.9), the linear growth rate is controlled by secondary nucleation and has a value ω_r.

The growth rate across the crystal surface (ω_s) is greater than the rate of formation of secondary nuclei (ω_i):

$$\omega_s \gg \omega_i \tag{6.66}$$

In this regime growth across the surface is assumed to occur as a monolayer until the whole of the substrate is covered. Monolayers are added to the substrate one by one and the linear growth rate (ω_r) is given by

$$\omega_r(\mathrm{I}) = biL \tag{6.67}$$

where b is the monolayer thickness, i is the surface nucleation rate, the number of nuclei per length of substrate per second, and L is the substrate length ($= n_s.a$, where n_s is the number of *stems* adsorbed onto the substrate and a is the *stem* width). Since iL is the rate of the formation of secondary nuclei on the substrate and b is the monolayer thickness, then a linear growth rate must be thus a product of iL and b. The total rate of crystallization, *i.e.* the total flux (S) of polymer crystallizing is

$$S_T = -Na \tag{6.68}$$

where N is the total number of *stems*, surface nuclei per unit time:

$$S_T = \left(\frac{1}{L_u}\right) \int_{2\sigma/\Delta g}^{\infty} S(L_c)\, \mathrm{d}L_c \tag{6.69}$$

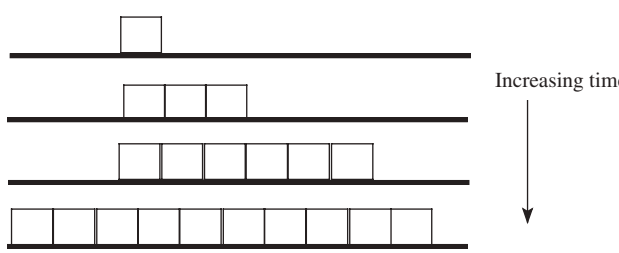

Figure 6.9 Regime I growth. The square boxes represent the cross-sections of the stems growing on the substrate.

where L_u is the length of the repeating unit. Combining eqn (6.68) and (6.69) gives

$$\omega_r(\mathrm{I}) = bS_T \frac{n_s}{N} \tag{6.70}$$

Integration of eqn (6.69) gives

$$S_T = \left(\frac{N_0\beta}{L_u}\right) P \exp\left(\frac{2ab\sigma\psi}{kT_c}\right) \exp\left(-\frac{4b\sigma\sigma_L}{\Delta G k T_c}\right) \tag{6.71}$$

where

$$P = RT_c\left[\frac{1}{2b\sigma_L - \psi ab\Delta G} - \frac{1}{2b\sigma_L - (1-\psi)ab\Delta G}\right] \tag{6.72}$$

Using the WLF equation for short-range diffusion factor (β):

$$\beta = \left(\frac{kT_c}{h}\right) J_1 \exp\left(-\frac{U^*}{R(T_c - T_\infty)}\right) \tag{6.73}$$

Finally combination of eqn (6.70)–(6.73) yields

$$\omega_r(\mathrm{I}) = \omega_{0r}(\mathrm{I}) \exp\left(-\frac{U^*}{R(T_c - T_\infty)}\right) \exp\left(-\frac{4b\sigma\sigma_L}{\Delta G k T_c}\right) \tag{6.74}$$

where

$$\omega_{0r}(\mathrm{I}) = b\left(\frac{kT_c}{h}\right) J_1 \exp\left(\frac{2ab\sigma\psi}{kT}\right) \tag{6.75}$$

Alternatively, using reptation to control the *stem* diffusion one obtains

$$\beta = \left(\frac{kT_c}{h}\right)\left(\frac{1}{M_z}\right) \exp\left(-\frac{\Delta E_r}{RT_c}\right) \tag{6.76}$$

where ΔE_r is the activation energy for reptation.

Regime II growth. As the temperature is lowered, multiple nucleation becomes possible and the condition for growth changes, *i.e.* $\omega_s < \omega_i$ (Figure 6.10), and the theory is modified accordingly to give the linear growth rate, $\omega_r(\mathrm{II})$:

$$\omega_r(\mathrm{II}) = b\sqrt{i\omega_s} \tag{6.77}$$

where ω_s is the growth rate across the crystal surface $= a\,(A - B)$ given by

$$\begin{aligned} \omega_s &= a\beta\left[\exp\left(-\frac{2ab\sigma}{kT_c} + \frac{\psi ab L_c \Delta G}{kT_c}\right) - \exp\left(-\frac{(1-\psi)ab L_c \Delta G}{kT_c}\right)\right] \\ &\approx a\beta \exp\left(-\frac{2ab\sigma(1-\psi)}{kT_c}\right) \end{aligned} \tag{6.78}$$

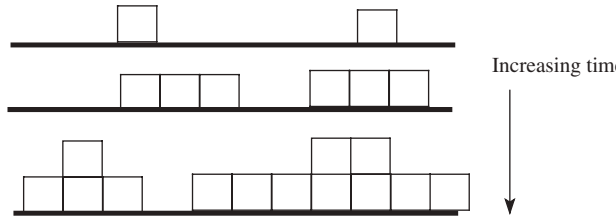

Figure 6.10 Regime II growth, showing that nucleation of a second layer occurs before the first is completed.

This expression is based on the concept that an isolated *stem* undergoes nucleation at time $t = 0$ and then grows equally in opposite directions. At a given time t, the length of the substrate covered by an additional monolayer is proportional to $2\omega_s.t$. The rate at which new nuclei form on this surface is $2\omega_s ti$, where i is the nucleation rate. The number of nuclei formed during the incremental time $\mathrm{d}t$ is given by

$$N(t)\mathrm{d}t = 2w_s ti\mathrm{d}t \tag{6.79}$$

The total number of nuclei formed during a time period t is

$$\int_0^t N(t)\,\mathrm{d}t \propto \int_0^t 2\omega_s it\,\mathrm{d}t = \omega_s it^2 \tag{6.80}$$

The average time $<t>$ to form a new nucleus to grow on the surface is

$$\omega_s i\langle t\rangle^2 \propto 1 \Rightarrow \langle t\rangle \propto \frac{1}{\sqrt{i\omega_s}} \tag{6.81}$$

The rate at which new layers are formed is given by

$$\omega_r(\mathrm{II}) = \frac{b}{\langle t\rangle} = b\sqrt{i\omega_s} \tag{6.82}$$

which is identical to eqn (6.77). Combining eqn (6.68), (6.71), (6.77) and (6.78) leads to an expression for the growth rate in regime II as:

$$\omega_r(\mathrm{II}) = \omega_{0r}(\mathrm{II})\exp\left(-\frac{U^*}{R(T_c - T_\infty)}\right)\exp\left(-\frac{2b\sigma\sigma_L}{\Delta G k T_c}\right) \tag{6.83}$$

where

$$\omega_r 0(\mathrm{II}) = b\left(\frac{kT_c}{h}\right)\exp\left(\frac{(2\psi - 1)ab\sigma}{kT_c}\right) \tag{6.84}$$

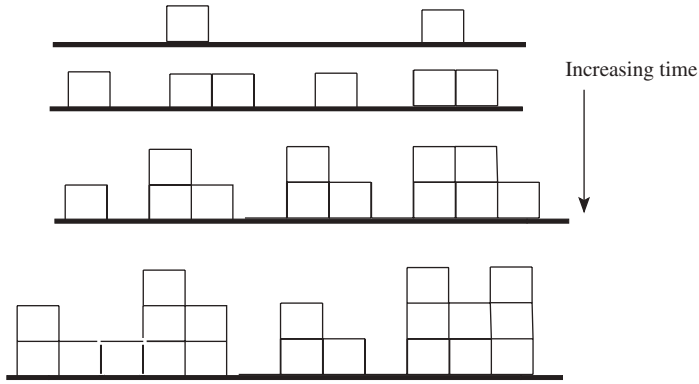

Figure 6.11 Regime III growth. The nucleation is faster than the growth across the surface and niches/grooves begin to be created.

Regime III growth. As the temperature is further lowered, prolific and multiple nucleation can occurs (Figure 6.11).

The niche separation becomes the same dimensions as the width of the *stem* and the growth rate, $\omega_r(\mathrm{III})$, is given by

$$\omega_r(\mathrm{III}) = biL \tag{6.85}$$

The growth rate in regime III may then be expressed by

$$\omega_r(\mathrm{III}) = \omega_{r0}(\mathrm{III}) \exp\left(-\frac{U^*}{R(T_c - T_\infty)}\right) \exp\left(-\frac{4b\sigma\sigma_L}{\Delta G k T_c}\right) \tag{6.86}$$

where $\omega_{r0}(\mathrm{III}) = C(kT_c/h)$ and the last exponent, which is the nucleation factor, is the same as that for regime I. The LH theory implies that as the melt is cooled so there will be changes in the dominant growth mechanism.

The changes in the rate are a consequence of the change in balance between free energy of the melt and that of the solid and its influence on the nucleation processes. The LH theory has been used extensively to analyse polymer crystal growth data and is able qualitatively to describe processes that occur in a number of polymer systems. Its success lies in its ability to describe the temperature dependence of both the initial crystal thickness (L_c^*) and the linear growth rate (ω_r). A large volume of data has been shown to fit the relationship:

$$L_c^* = \frac{C_1}{\Delta T} + C_2 \tag{6.87}$$

and

$$\omega_r = \beta \exp\left(-\frac{K_g}{T_c \Delta T f}\right) \tag{6.88}$$

where C_1, C_2, K_g and f are constants. Plots of $\log(G)/\beta$ as a function of $1/T_c\Delta T$ consist of lines with relatively abrupt changes in the slope coefficients as

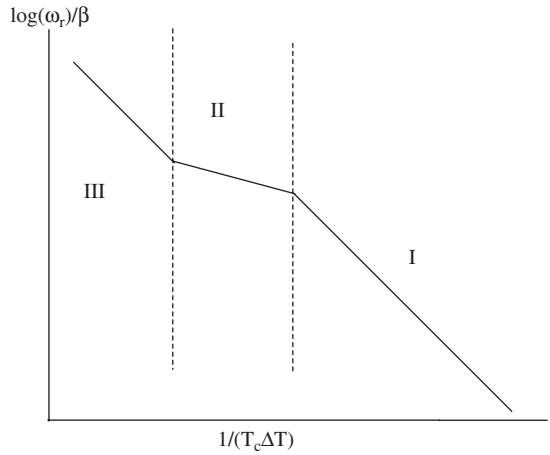

Figure 6.12 Schematic of the predictions of the LH theory for polymer crystal growth.

indicated in Figure 6.12. The growth rate exhibits approximately linear behaviour between the transitions from one regime to another.

The above equations can be simplified if we use

$$\begin{aligned}\Delta G &= \Delta H^0 - T_c \Delta S = \Delta H^0 \left[1 - \frac{T_c}{T_m^0}\right] \\ &= \frac{\Delta H^0}{T_m^0}\left[T_m^0 - T_c\right] = \frac{\Delta H^0 \Delta T}{T_m^0}\end{aligned} \tag{6.89}$$

and insertion of eqn (6.88) into the rate equations (6.74), (6.83) and (6.86) allows calculation of various constants for the crystallization process in the expression for K_g shown in Table 6.3.

The transition from regime I to regime II crystallization was reported[25] as being sharp and accompanied by a distinct change in supermolecular structure from axialitic to spherulitic. The LH theory predicts[24] that the ratio of the slopes (K_g) in regimes I and II growth regions is 2:1. The transition from regime I to regime II can be predicted by the so-called Z test.[28] The quantity Z is defined by

$$Z = \frac{\omega_i L^2}{4\omega_s} \tag{6.90}$$

where L is the length of the substrate, and estimated using eqn (6.90) has been ascribed values of the order of 0.1 μm. Regime I occurs when $Z < 0.1$ and regime II when $Z > 1$. Although there is no doubt that these transitions occur, whether the simple growth processes described by theory are always applicable is a matter of debate. Diffusion is an important factor in the crystallization process and to some extent is allowed for by the incorporation of the reptation

Table 6.3 Growth rate equations and growth rate data for linear polyethylene.[4,24]

	Regime I	*Regime II*	*Regime III*
K_g [a]	$\frac{4b\sigma\sigma_L}{\Delta H^0 k}$	$\frac{2b\sigma\sigma_L}{\Delta H^0 k}$	$\frac{4b\sigma\sigma_L}{\Delta H^0 k}$
ΔT (K)	<17	17–23	>23
ω_s/ω_i	$\gg 1$	< 1	$\ll 1$
Supermolecular structure	Axialitic	Spherulitic	Spherulitic

[a] $\omega_r = \beta \exp(-K_g/T_c \Delta T f)$; units of K_g are those of ΔH^0 (J m^{-3}).

theory in the above description. The most contentious issue is whether the folds are tight or random.[29,30] As we will see later, the possibility of rearrangement involving the *stems* changing their conformation on the surface has to be a possibility and aids the formation of tight folds. Determination of the value of L has also been a point of uncertainty. Using decoration techniques the persistence length, which is the average distance between adjacent secondary nucleation sites, has been determined to have a maximum value of 200 nm,[31–33] which is a significantly lower value than would be predicted by the LH theory.

The persistence length is determined by the ratio of the growth rate (ω_s) across the surface to the secondary nucleation rate (ω_i). The LH theory predicts a change in the growth rate because ω_s is weakly temperature dependent whereas ω_i is strongly dependent. Alternative explanations for changes in rate have been put forward and include effects such as the temperature dependence of the interfacial energies, viscosity effects and nucleation processes.

6.9.2 Sadler–Gilmer Theory

In Chapter 2 it was pointed out that the shape, or *habit*, of a crystal depended on growth mechanism and required consideration of the frequency of occurrence of various defects being created in the crystal surface. A temperature exists, the roughening temperature (T_r), at which growth occurs from the defects; below this temperature growth occurs at the facets as discussed in Chapter 2. When crystallization of polyethylene is carried out at higher temperatures and in poorer solvents, single crystals with slightly rounded {100} sectors are obtained. Crystallization at very high temperatures leads to leaf-shaped crystals.

In the case of the crystallization of low molecular mass materials at temperatures above T_r, the growth is proportional to ΔT, whereas experiments on crystal growth in the case of polymers indicate that the growth rate is proportional to $1/T_c \Delta T$. Sadler[34] suggested that the difference in temperature dependence above T_r was of an entropic origin. In colloid science entropic barriers as a

consequence of a distribution of chain conformations are well known and are discussed in Chapter 11.

The Sadler–Gilmer theory[26] leads to a prediction of the growth rate:

$$\omega_r \propto \exp\left(-\frac{K_g}{T_c \Delta T}\right) \quad \text{and} \quad L_c^* = \frac{C}{\Delta T} + \delta L_c \tag{6.91}$$

which is in agreement with experiment. If the absorption energy of the *stem* onto the surface is large compared with kT then roughening will not occur. If it is assumed that rather than the whole *stem* adding as a single step, only part of the *stem* adds to the surface and the remainder then collapses behind it then roughening becomes possible. A short element of six CH_2 units would have an interaction energy of approximately $0.6kT$ and attachment of such a short section would allow roughening. The attachments can be divided into various forms: 'blind attachment', 'pinning' and 'detachment'.[4] Polymer chains in the melt will have a variety of different conformations depending on the temperature. As the temperature is lowered so linear all-*trans* elements will be favoured; a chain that has a particular conformation in the melt becomes attached to the surface but its conformation is not necessarily suitable for later stages of crystal growth. The *stem* length may lie below the limit of thermodynamic stability allowing the chain to become detached from the site. There is clearly a critical length of the all-*trans* element for stable attachment to occur but this may also incorporate chain folds and/or loops that can prohibit further growth. For growth to continue either this element has to become detached or this unfavourable conformation has to change into a more favourable conformation. The Sadler–Gilmer theory incorporates the possibility of dynamic exchange of the type depicted in Figure 6.13.

The dynamics of this process are encapsulated in the Sadler–Gilman model[26] that considers the balance between the forward and backward reactions in terms of the ratio k_-/k_+:

$$\frac{k_-}{k_+} = \exp\left(\frac{2\varepsilon}{kT_m^0} - \frac{m\varepsilon}{kT_c}\right) \tag{6.92}$$

where ε is the interaction energy, m is the number of neighbouring sites, T_m^0 is the equilibrium melting point and T_c is the crystallization temperature. As with other theories in polymer science, the connectivity of the chain elements influences the allowed possible ways in which attachment and detachment can occur. The statistical mechanical analysis has to be constrained to consider only those chains that exist at the surface. Two different methods have been used to derive kinetic expressions. The first approach sets up the rate equations for the various steps and solves these numerically and provides averaged values of the various constants. The second approach uses Monte Carlo simulation and allows the growth process to be mapped in time[26,35] and is in good agreement with experiment.

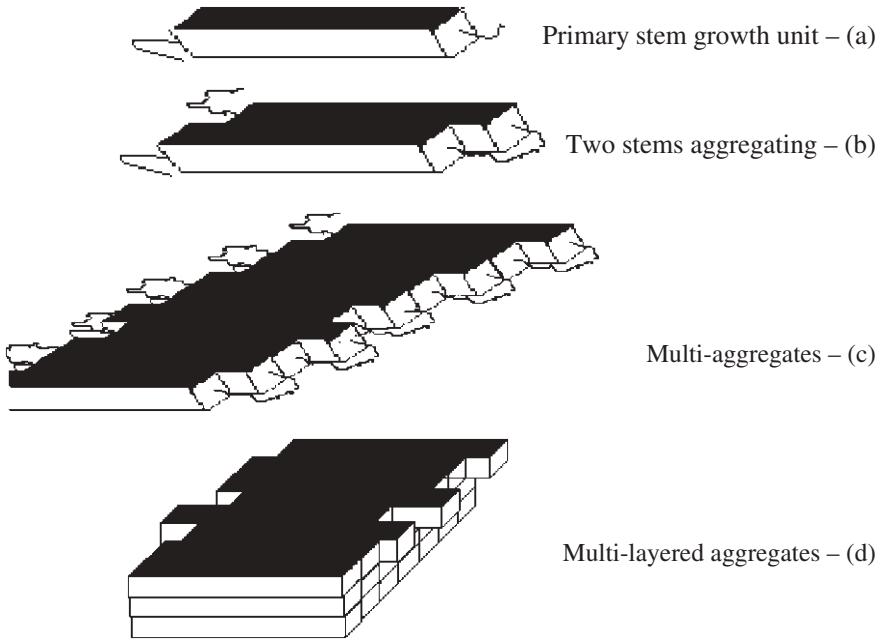

Figure 6.13 The building of a crystal surface; (a) primary stem with disordered cha9ns at each end. There will be a distribution of stem lengths. (b) aggregation of two stems, (c) multli aggregates, and (d) multilayered stems.

6.10 Crystallization via Metastable Phases

In Chapter 4, the plastic crystalline phase of low molar mass hydrocarbons was discussed. Just below the melting point a high degree of rotational freedom is observed whilst restricting the molecules to a defined lattice structure. In polyethylene, studies at elevated pressure have identified the existence of a stable hexagonal structure rather than the usual orthorhombic structure. This hexagonal phase allows rapid crystal thickening and the formation of extended chain crystals without any chain folds. The thickening in the case of the orthorhombic phase crystals is a considerably slower process, but does also occur. In both cases, the folds change to all-*trans* structures and signify the ability for the polymer crystal at elevated temperatures to undergo dynamic changes. The nature of these dynamic changes has been studied using a variety of methods.

Potential impact of rotator phase on crystallization. Molecular dynamics simulations[35] have been carried out to study the conformational defects in the orientationally ordered structures of short-chain molecules and polymer chains. The simulation showed the creation of orientationally ordered structures from a random coil configuration by cooling from the melt. The longer chains exhibit folding with double *gauche* defects with the same sign (. . . tg(+)g(+)t . . .) predominantly located at the chain ends and the kink defects (. . . tg(+)tg(−)t . . .), which do not cause serious deformation of

chain molecules, can exist even at the chain interiors. On the other hand, in the case of a single polymer chain, several types of the conformational defects which give rise to large deformation of a polymer chain, such as the double *gauche* defects with opposite sign (. . . tg(+)g(−)t . . .), can be observed in the fold surfaces. A number of similar calculations have been reported,[36–45] all demonstrating that it is possible to incorporate in the simulations subtle effects which allow better comparison between experiment and theory. Changes in the force field allow a level of disorder to be include which is consistent with the slight deviations in lattice parameters observed experimentally.[36] Calorimetric studies of homogeneous nucleation of crystallizing *n*-alkanes (CH_3–$(CH_2)_{n-2}$–CH_3), with values of n which lie between 17 and 60 and low molar mass polyethylene fractions have indicated that the surface energy varies for *n*-alkanes as low as $n = 25$ which is below the value that is normally considered to be the lower limit for chain folding. This behaviour is consistent with the entropic model, in which the surface energy increases when the 'cilia' dangling from the bundle nucleus exceed a length where their entropic cost begins to raise significantly the surface energy. At low n, homogeneous nucleation occurs into the metastable rotator phase that plays a significant role in the nucleation process.[38] A number of studies have examined the potential influence of the rotator phase and conclude that it plays a significant role in the growth process for medium to high molecular weight polymers and may also be evident in low molecular mass materials.[39–45]

Behaviour of other polymer systems. The important of metaphases in the crystallization of *trans*-poly(1,4-butadiene) has a been observed.[46] The polymer can exist in two forms, a monoclinic phase stable at low temperatures and a hexagonal phase that is stable at high temperatures and similar to the hexagonal phase of polyethylene. In heating *trans*-poly(1,4 butadiene) at normal pressure, a transition from monoclinic to hexagonal structure occurs and rapid crystal thickening is observed. Keller *et al*.[47] have suggested that this behaviour may be common to other polymer systems. Crystallization proceeds through the mobile hexagonal phase that permits rapid crystal thickening, with the orthorhombic phase being formed when the crystals reach a certain critical thickness and applies to melt crystallization of polyethylene at normal pressure.

6.11 Molecular Fractionation

Separation of small molecules into different phases is a well-known phenomenon.[48] Polymers that have a different molar mass have sufficient free energy difference to have a tendency to separate and differences in their melting points will allow fractionation into different crystalline species. Lower molar mass materials will crystallize at low temperatures into separate lamellae often located between the dominant lamellae or at the spherulite boundaries.[19,49] At each crystallization temperature there will exist a critical molar mass (M_{crit}) such that the molecules of molar mass greater than M_{crit} are able to crystallize at this temperature whereas molecules of molar mass less than M_{crit} are unable

to crystallize. Fractionation has been demonstrated for a range of polymer systems.[50,51] The equilibrium melting point of a given polymer is dependent not only on its molar mass but also on the molar masses of the other species present in the melt:[19]

$$\frac{1}{T_m} - \frac{1}{T_m^0(M)} = \frac{R}{\Delta H}\left[-\ln \nu_p + (x-1) \times (1-\vartheta_p) - x\chi(1-\nu_p)^2\right] \tag{6.93}$$

where T_m is the melt temperature, $T_m^0(M)$ is the equilibrium melting crystallization temperature of the pure species of molar mass M, R is the gas constant, v_p is the volume fraction in the melt of the crystallizing species, ΔH is the molar heat of fusion, χ is the interaction parameter and $x = \sum v_i x_i / \sum v_i$ is the volume fraction of the crystallizing species with respect to all other polymers in the melt. The validity of this expression has been shown experimentally. Mehta and Wunderlich[19] have suggested that a particular species nucleates separately and it is the size of this nucleus that governs the growth. Polymers with branched chain structure and differences in tacticity exhibit not only molar mass segregation but also segregation according to structural type. The crystallization temperature is shifted towards lower temperatures with increasing degree of chain branching.

Blends of linear and branched polyethylene normally crystallize in two stages. The components crystallize separately provided that they are of similar molar mass. Linear polyethylene will crystallizes at the highest temperatures, forming regular shaped crystal lamellae. Branched polymers crystallize at lower temperatures in finer, S-shaped lamellae located between the stacks of the dominant lamellae. Although linear and branched polyethylenes are chemically very similar they can phase separate in the molten state.[52] A characteristic of phase separated behaviour is the observation of a dominant lamella structure (Figure 6.14).[53–55]

Metallocene polymers. Since the mid-1990s vinyl polymers synthesized using metallocene catalysts have been commercially available. These polymers have 'purer' structures than those previously available produced using Zeigler–Natta polymerization methods. The characteristics of metallocene polymers are that they can have a very low density of chain defects (side chains) and very narrow molecular mass distributions. Such materials conform very closely to ideal linear polymers and they exhibit many of the classic characteristics expected of such polymers. Metallocene polymers will often have incorporated small amounts of a monomer with a side chain to control the degree of crystallinity. The distribution of these side chains is often much more regular than in the case of the Zeigler–Natta materials and this is reflected in the type of crystalline structure generated. Because the materials are stereochemically and molar mass well defined they exhibit fractionation on slow cooling. This is demonstrated by the DSC analysis of the cooling behaviour. Two distinct peaks are observed for polymers that have molar masses below the critical value for entanglement and reflect the creation of different types of lamellar structures (Figure 6.15). The highest temperature peak at 116 °C reflects the lamellae formed from the

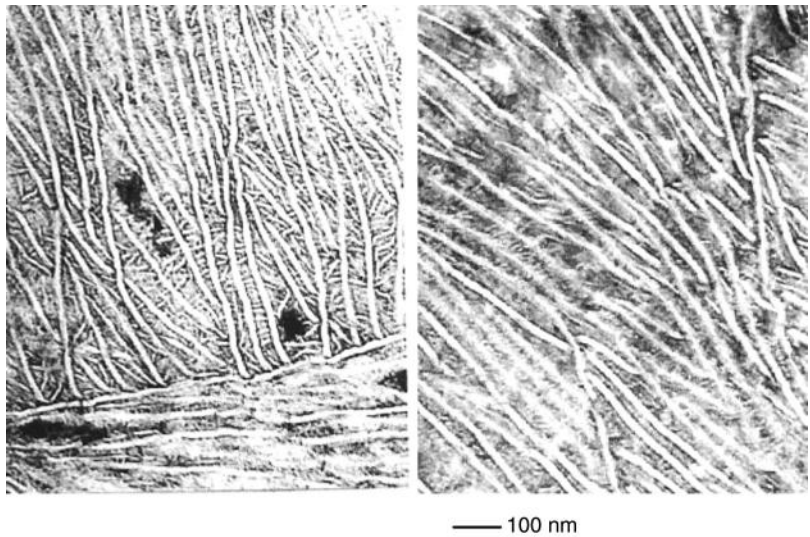

Figure 6.14 Transmission electron micrographs of a polyethylene blend.[57]

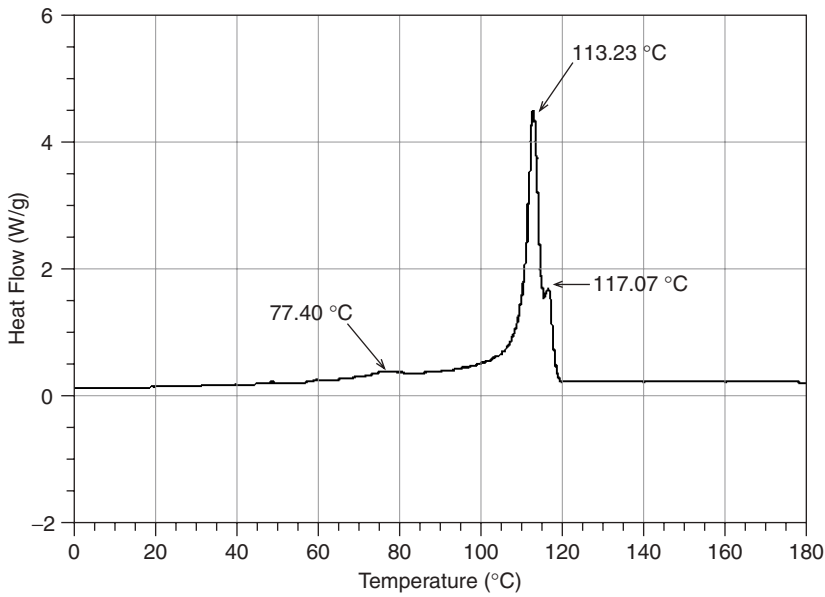

Figure 6.15 DSC trace for metallocene polyethylene indicating multiple melting points.

dominant molar mass species and this forms the main lamellar structure. The secondary structure is associated with the lower melting peak at 112.5 °C. Lower mass fractions form a broad low melting peak at ~77 °C and corresponds to the small crystallites that infill between the lamellae.

Various electron microscopy studies[56] of these materials have shown that very large lamellar structures are observed and that axialitic growth is dominant. The chains fold and add to the lamellae in an ordered fashion to create these large structures. The lamellae have very few bridging *tie* chains and this is evident in the poor environmental stress crack resistance of the materials. If the molar mass is increased above M_c the growth becomes more spherulitic and the lamellae are connected by an increasing number of tie molecules and the environmental stress crack resistance is dramatically improved. There is a very close connection between the morphology generated in the solid state and the bulk mechanical properties.[57]

6.12 Orientation-Induced Crystallization

Many polymers when extruded or in some other way subjected to an external force, which has an impact on the material alignment, exhibit an enhanced degree of crystallinity. The external forces can shear the polymer chains leading to elongation in the direction of the flow. The extent to which alignment is achieved will depend on the rate of oscillation or shear rate to which the melt is subjected. A balance between the natural Brownian motion and the applied forces that attempt to achieve alignment determines the configuration that the polymer chain adopts. The relaxation of the polymer in the melt is well understood and is describe by a combination of Rouse and reptation motion.[58] Reptation motion is only observed for polymers with molecular mass above the critical value for entanglement (M_c) and is several orders of magnitude slower than for the collective motions of the chain described as the Rouse modes. Subjecting a high molar mass polymer can induce alignment and elongation in the flow direction that will place the chain elements in a more favourable position thermodynamically to be able to crystallize. Rubber elasticity theory similarly allows the thermodynamic state of the molecule to be related to the degree of extension in the melt.[59–61] The process which occurs is closely related to that of strain hardening observed when melts are subjected to uniaxial elongational flow.[62] In rubber elasticity theory the degree of extension is connected to the free energy through the entropy. Using this approach the equilibrium melting point is defined by

$$T_m^0 = \frac{H_m - H_c}{S_m - S_c} = \frac{\Delta H^0}{S_m^0 - (R/2)\left[\lambda^2 + (2/\lambda) - 3\right] - S_c^0} = \frac{\Delta H^0}{\Delta S^0 - (R/2)\left[\lambda^2 + (2/\lambda) - 3\right]} \tag{6.94}$$

where λ is the molecular 'draw ratio', which is the ratio of the size of the chain in the flow field to that in the absence of the flow field, R is the gas constant and ΔH^0 and ΔS^0 are, respectively, the enthalpy and entropy changes between the melt and the crystalline state. The second term in the denominator in eqn (6.94)

comes from the statistical mechanical theory of rubber elasticity. The effective degree of supercooling at a given crystallization temperature (T_c) increases due to orientation:

$$\Delta T = \Delta T_m - \Delta T_c = \frac{\Delta H^0}{\Delta S^0 - \frac{R}{2}\left(\lambda^2 - \frac{2}{\lambda} - 3\right)} - T_c$$

$$= \frac{\Delta H^0}{\Delta S^0}\left[\frac{\Delta S^0}{\Delta S^0 - \frac{R}{2}\left(\lambda^2 + \frac{2}{\lambda} - 3\right)}\right] - T_c$$

$$T_m^0(\lambda = 1)\left[\frac{1}{1 - \frac{(R/2)\left[\lambda^2 - (2/\lambda) - 3\right]}{\Delta S^0}}\right] - T_c \tag{6.95}$$

The kinetics of orientation-induced crystallization has been studied by a number of researchers who have combined the above with the Avrami equation and shown that this approach provides an acceptable description of the processes that occur. Molecular simulations[63] of uniaxial ordering and creation of a ribbon-like polymer structure depend on the effective energy of interaction between the polymer and the flow field. The transition temperature depends on the polymer chain length, decreasing linearly with the reciprocal of the length for chains containing more than 100 monomer units. On the other hand, the change of the entropy is independent of the polymer length for molecules containing more than 30 monomers. This prediction and also calculations based on the Doi–Edwards[64] model for reptation provide good agreement with experimental data.[65] The influence of entanglement and the creation of the amorphous domain can be predicted by consideration of the frequency of the occurrence of entanglements and the associated relaxation rates for disentanglement. The predictions are close to experiment.[66]

Recommended Reading

D.C. Bassett, *Principles of Polymer Morphology*, Cambridge Solid State Series, Cambridge University Press, Cambridge, 1981.
U.W. Gedde, *Polymer Physics*, Chapman and Hall, Glasgow, 1995.
A. Keller and G. Goldbeck-Wood, in *Comprehensive Polymer Science, Supplement 2*, ed. G. Allan, Pergamon Press, Oxford, 1996.
A.S. Vaughan and D.C. Bassett, in *Comprehensive Polymer Science*, ed. G. Allen, Pergamon Press, Oxford, 1989, vol. 2.

References

1. P.J. Flory, *Statistical Mechanics of Chain Molecules*, Interscience, New York, 1969.
2. A. Keller, *Philos. Mag.*, 1957, **2**, 1171.

3. P.J. Barham, R. Chivers, A. Keller, J. Matinez-Salazar and S. Organ, *J. Mater. Sci.*, 1985, **20**, 1625.
4. U.W. Gedde, *Polymer Physics*, Chapman & Hall, 1995, ch. 8.
5. J.I. Lauritzen Jr and J.D. Hoffman, *J. Res. Natl Bur. Std.*, 1960, **64A**, 73.
6. L. Mandelkern, *Physical Properties of Polymers*, American Chemical Society, Washington, DC, 1984, p. 155.
7. G. Ungar, J. Stejny, A. Keller, I. Bidd and M.C. Whiting, *Science*, 1985, **229**, 386.
8. P. Spegt, *Makromol. Chem.*, 1970, **139**, 139.
9. P.H. Geil, F.R. Anderson, B. Wunderlich and T. Arakawa, *J. Polym. Sci. A*, 1964, **2**, 3707.
10. D.C. Bassett, S. Block and G.J. Piermarini, *J. Appl. Phys.*, 1974, **45**, 4146.
11. P.J. Flory, *J. Am. Chem. Soc.*, 1962, **84**, 2857.
12. D. Sadler, in *Crystalline Polymers*, ed. I. H. Hall, Elsevier, Amsterdam, 1984.
13. J.S. Higgins and H.C. Benoit, *Polymers and Neutron Scattering*, Clarendon Press, Oxford, 1994, p. 268.
14. S.J. Spells, A. Keller and D.M. Sadler, *Polymer*, 1984, **25**, 749.
15. B. Wunderlich, *Macromolecular Physics*, Academic Press, New York/London, 1973, vol. 1.
16. D.C. Bassett, *Principles of Polymer Morphology*, Cambridge University Press, Cambridge, 1981.
17. M.L. Williams, R.F. Landel and J.D. Ferry, *J. Am. Chem. Soc.*, 1955, **77**, 3701.
18. B. Wunderlich, *Macromolecular Physics: 3. Crystal Melting*, Academic Press, New York, 1980. pp. 72–73.
19. A. Mehta and B. Wunderlich, *Colloid Polym. Sci.*, 1975, **253**, 193.
20. B. Wunderlich, *Macromolecular, Physics: 2, Crystal Nucleation Growth Annealing*, Academic Press, New York/London, 1978.
21. B. Wunderlich and A. Mehta A, *J. Polym. Sci., Polym. Phys. Ed.*, 1974, **12**, 255.
22. A.J. Kovacs, *Ric. Sci. (Suppl.)*, 1955, **25**, 668.
23. E. Ergoz, J.G. Fatou and L. Mandelkern, *Macromolecules*, 1972, **5**, 147.
24. J.D. Hoffman and R.L. Miller, *Macromolecules*, 1988, **21**, 3038.
25. J.D. Hoffman, L.J. Frolen, G.S. Ross and J.I. Lauritzen Jr, *J. Res. Natl Bur. Std. A. Phys. Chem.*, 1975, **79A**, 671.
26. D.M. Sadler and G.H. Gilmer, *Polymer*, 1984, **25**, 1446.
27. P.G. De Gennes, *J. Chem. Phys.*, 1971, **54**, 5143; *J. Chem. Phys.*, 1971, **55**, 572.
28. J.I. Lauritzen Jr, *J. Appl. Phys.*, 1973, **44**, 4353.
29. J.D. Hoffman, C.M. Guttman and E.A. DiMarzio, *Discuss. Faraday Soc.*, 1979, **68**, 177.
30. D.Y. Yoon and P.J. Flory, *Polymer*, 1977, **19**, 509.
31. J.J. Point, M.C. Colet and M. Dosiere, *J. Polym. Sci. Polym. Phys. Ed.*, 1986, **24**, 357.
32. J.J. Point and M. Dosiere, *Polymer*, 1989, **30**, 2292.
33. J.J. Point and D. Villars, *Polymer*, 1992, **33**, 2263.

34. D.M. Sadler, *Polymer*, 1983, **24**, 1401.
35. G. Goldbeck-Wood and D.M. Sadler, *Mol. Simul.*, 1989, **4**, 15.
36. S. Fujiwara and T. Sato, *Prog. Theor. Phys. Suppl.*, 2000, **138**, 342.
37. T.L. Phillips and S. Hanna, *Polymer*, 2005, **46**, 11003.
38. H. Kraack, M. Deutsch and E.B. Sirota, *Macromolecules*, 2000, **33**, 6174.
39. T.L. Phillips and S. Hanna, *Polymer*, 2005, **46**, 11035.
40. M.J. Nowak and S.J. Severtson, *J. Mater. Sci.*, 2001, **36**, 4159.
41. P.K. Mukherjee and M. Deutsch, *Phys. Rev. B*, 1999, **60**, 3154.
42. K. Nozaki and M. Hikosaka, *J. Mater. Sci.*, 2000, **35**, 1239.
43. E.B. Sirota and A.B. Herhold, *Polymer*, 2000, **41**, 8781.
44. S. Fujiwara and T. Sato, *J. Chem. Phys.*, 2001, **114**, 6455.
45. I.E. Mavrantza, D. Prentzas, V.G. Mavrantzas and C. Galiotis, *J. Chem. Phys.*, 2001, **115**, 3937.
46. S. Rastogi and G. Ungar, *Macromolecules*, 1992, **25**, 1445.
47. A. Keller, M. Hikosaka, S. Rastogi, A. Toda, P.J. Barham and G. Goldbeck-Wood, *J. Mater. Sci.*, 1994, **29**, 2579.
48. R. Koningsveld, W.H. Stockmayer and E. Nies, *Polymer Phase Diagrams: A Text Book*, Oxford University Press, Oxford, 2001.
49. M.I. Bank and S. Krimm, J. Polym. Sci., *Polym. Lett.*, 1970, **8**, 143.
50. X.H. Guo, B.A. Pethica, J.S. Huang and R.K. Prud'homme, *Macromolecules*, 2004, **37**, 5638.
51. X.H. Guo, B.A. Pethica, J.S. Huang, R.K. Prud'homme, D.H. Adamson and L.J. Fetters, *Energy Fuels*, 2004, **18**, 930.
52. P.J. Barham, M.J. Hill, A. Keller and C.C.A. Rosney, *J. Mater. Sci. Lett.*, 1988, **7**, 1271.
53. M. Conde Brana and U.W. Gedde, *Polymer*, 1992, **33**, 3123.
54. U.W. Gedde, *Prog. Colloid Polym. Sci.*, 1992, **87**, 8.
55. A.E. Woodward, *Atlas of Polymer Morphology*, Hanser, Munich/Vienna/New York, 1989.
56. A.J. Muller, M.L. Arnal, A.L. Spinelli, E. Canizales, C.C. Puig, H. Wang and C.C. Han, *Macromol. Chem. Phys.*, 2003, **2004**, 1497.
57. J.H. Magill, *J. Mater. Sci.*, 2001, **36**, 3143.
58. R.T. Bailey, A.M. North and R.A. Pethrick, *Molecular Motion in High Polymers*, Oxford University Press, 1981.
59. H. Janeschitz-Kriegl, *Prog. Colloid Polym. Sci.*, 1992, **87**, 117.
60. G. Eder, H. Janeschitz-Kriegl and S. Liedauer, *Prog. Colloid Polym. Sci.*, 1992, **87**, 129.
61. J.M. Haudin and N. Billon, *Prog. Colloid Polym. Sci.*, 1992, **87**, 132.
62. C. Gabrial and H. Munstedt, *J. Rheol.*, 2003, **47**(3), 619.
63. A.E. Arinstein, *Phys. Rev. E*, 2005, **72**, 51806.
64. M. Doi and S.F. Edwards, *The Theory of Polymer Dynamics*, Clarendon Press, Oxford, 1986.
65. S. Coppola, N. Grizzuti and P.L. Maffettone, *Macromolecules*, 2001, **34**, 5030.
66. K. Iwata, *Polymer*, 2002, **43**, 6609.